NASA Technical Memorandum 85759

NASA-TM-85759 19840010138

RECONFIGURABLE MULTIVARIABLE CONTROL LAW FOR COMMERCIAL AIRPLANE USING A DIRECT DIGITAL OUTPUT FEEDBACK DESIGN

Aaron J. Ostroff and Richard M. Hueschen

February 1984

National Aeronautics and Space Administration

Langley Research Center
Hampton, Virginia 23665

CONTENTS

SUMMARY

The ability of a pilot to reconfigure the control surfaces on an airplane after a failure, allowing the airplane to recover to a safe condition for landing, becomes more difficult with increasing airplane complexity. Techniques are needed to stabilize and control the airplane immediately after a failure, allowing the pilot time to make longer range decisions. This paper shows a design of a discrete multivariable control law using four controls for the longitudinal channel of a B-737, allowing redundancy in two of the three airplane rigid body degrees of freedom. Single control element failures are allowed in three of the four controls. The four controls design and failure cases are analyzed by means of a digital airplane simulation, with regard to tracking capability and ability to overcome severe windshear and turbulence during the approach and landing phase of flight.

INTRODUCTION

As future commercial airplanes become more sophisticated, the advent of unanticipated control element failures become more probable and will be more difficult to resolve. Future airplanes are expected to have reduced static stability and some may be staticaly unstable. There has been, and will continue to be, a proliferation of control surfaces. Primary control elements are taking on secondary functions (ref. 1) and in the future, primary control surfaces will probably be split into independently controlled surfaces. Automatic control systems will have increased complexity and capabilities such as fly-by-wire (FBW) systems (ref. 2,3).

With all of this capability, there are an unlimited number of ways things can go wrong, but only a sub-set of the failures can be anticipated with pre-planned specified procedures. There is a need to have a capability to automatically restructure the control laws of highly augmented airplanes to allow safe operation in the presence of unanticipated failures. Recent theoretical developments address some key elements of the overall restructurable control problem, a problem that is highly nontrivial and very important, but additional problem focused research is required (ref. 4).

A significant amount of progress has been made in fault tolerant areas related to sensors (redundancy management and analytical redundancy) and computers (self test procedures and designs). A major remaining reliability bottleneck is the control surface element failures (ref. 5). With recent advances in modern control theory, it is appropriate to investigate fault tolerant approaches to accommodate control surface failures. Reconfigurable control law research has recently been documented with respect to military airplanes (ref. 6,7), but as yet no related work has been reported for commercial airplanes.

For the research reported on in this paper, it is assumed that the sensors and computers are fully operational and that a failure occurs only in a control surface element. The objective of this research is to design a control law that allows the airplane to recover to a safe landing, even though

performance may be degraded. This present objective is for a reconfigurable control law design, which contrasts to the long term objective of a restructurable control law design, i.e., to automatically design the new control law on the airplane after detecting and identifying (FDI) the failure. A further assumption for this paper is that the FDI process supplies perfect information to the control logic.

AIRPLANE MODEL AND CONTROL LAW STRUCTURE

A B-737 airplane is used for the preliminary longitudinal control channel design since stability and control data, as well as a full six degree-of-freedom nonlinear simulation, is available at LaRC. In the existing airplane, the stabilizer position is dependent upon the elevator position and the spoilers can only be controlled automatically in the lateral-directional channel. However, for this study, it is assumed that four independent controls are available: throttle, stabilizer, elevator, and spoilers.

A PIF/CGT (proportional-integral-filter with command generator tracking) discrete control structure was selected for the reconfigurable control law because of properties that are appropriate for the task (ref. 8-15). PIF is a direct digital integrated formulation using linear dynamics for design. All control signals are rate-commands and the change from rate to control position-commands accommodate necessary computation delays. Proportional feedback of control position-commands allows additional filtering properties in each control channel. Only measurable states are being fed back and selected outputs are integrated to give type 1 control properties. Some of the integrated states are command tracking errors which are penalized in the cost function independent of the command model chosen.

The command generator uses an output model following approach to emulate specific objectives, such as changes in altitude and velocity. Feedforward gains, connecting the command model to the control inputs, are calculated open loop, independent of the feedback gains.

All equations are implemented in incremental form using total measurable quantities. This implementation has been shown to work well with nonlinear dynamics (ref. 13,14,15). Trim values are not needed in flight, as the airplane goes to a new equilibrium state as a function of slowly varying commands. Automatic trim capability is very important, and for many cases the control problem would be solved if trim can be established (ref. 16).

The PIF/CGT structure has been combined with a stochastic discrete optimal output feedback formulation, for time invariant plants (ref. 17). Both proportional outputs and integral outputs are selected for the output feedback gains. A research effort that used the output feedback formulation and included constrained dynamic compensation is given in Reference 18.

DESIGN EXAMPLE

The longitudinal channel of a B-737 is used as the design case for the

reasons presented in the previous section. The design assumes four independent controls: throttle δ_{th} stabilizer δ_s, elevator δ_e, and spoilers δ_{sp} biased at eight degrees. First order low frequency actuator dynamics are assumed for the δ_{th} and δ_s channels, while the other two channels are assumed to have a fast response compared to the frequencies of interest. All results shown are based upon a point design for a three degree glideslope, airspeed V_a of 215 ft/s (127 Kt), weight 85,000 lbs., and CG equal to a 0.2 mean aerodynamic chord. The mathematical formulation for the design example is given in Appendix A.

Output Feedback Gains

The design example for perturbation equations (A1) and (A2) include 15 states ($\Delta\bar{x}$), 4 control rate-commands (Δv) and 13 outputs ($\Delta\bar{y}$). Components of the 15 PIF states and 13 outputs are

$$\Delta x = \left[\Delta U, \Delta W, q, \theta, \Delta Z, \Delta X\delta_t, \Delta X\delta_s\right]^T \quad (1)$$

$$\Delta u = \left[\Delta\delta_{th}, \Delta\delta_s, \Delta\delta_e, \Delta\delta_{sp}\right]^T \quad (2)$$

$$\Delta z = \left[\int\Delta Z dt, \int\Delta V_a dt, \int\Delta\delta_e dt, \int\Delta\delta_{sp} dt\right]^T \quad (3)$$

$$\Delta\bar{y} = \left[\Delta V_a, \Delta\dot{Z}, q, \Delta\theta, \Delta Z, \Delta\delta_{th}, \Delta\delta_s, \Delta\delta_e, \Delta\delta_{sp}, \Delta z(1), \Delta z(2), \Delta z(3), \Delta z(4)\right]^T \quad (4)$$

where $\Delta z(i)$ represents the i^{th} integrator state in equation (3), $\Delta U, \Delta W$ are body axis inertial velocity perturbation components, q is the pitch rate, $\Delta\theta$ is the pitch attitude perturbation, ΔZ is the altitude error, $\Delta X\delta_t$, $\Delta X\delta_s$ are states for the first order throttle and stabilizer dynamics, $\Delta\dot{Z}$ is the altitude rate perturbation, and all other variables have previously been defined. The 4 control rate-commands are the time differentials of the 4 components in equation (2).

Appendix B includes the weighting approach with the corresponding weightings used in the peformance index and the optimal output feedback gains K used for the design example. Also included in this appendix are the command generator models with the associated feedforward gains. The closed loop eigenvalues (S) and damping ratios (ζ), calculated by inserting K into equation (A16), are shown for the 4 controls case in Table I. The first two complex eigenvalues represent the phugoid and short period modes respectively, and are shown next to the corresponding eigenvalues for the open loop plant. Bode data for the equivalent case is shown in the lower part of Table I, and includes the phase margin P_M and gain margin G_M at the corresponding radian frequency ω. Bode data is obtained by opening each control channel separately at the control position-command input (Δu). Figure 1 shows the Bode plots for each of the four control channels. All gain margins are better than the 6 db classical design value, and only the δ_{th} loop phase margin is somewhat less than 60 degrees.

Failure detection and identification (FDI) is assumed operational with perfect information supplied to the control logic. An objective of the failure cases is to determine if a subset of the existing feedback gains can be used to maintain a safe flight condition, even though performance may be

degraded. The failure cases considered represent single failures in either the stabilizer, elevator, or spoiler control element. The throttle channel was not analyzed at this time since complete loss of thrust represents a noncontrollable case. The loss of one engine requires cross coupling derivatives and will be considered in the future.

For each control element failure, a reconfigured control law is used, whereby, one row and two columns of K are set equal to zero. The nulled row corresponds to one of the failed control rate-commands (see eq.A15) one nulled column corresponds to one of the control position-command states (see eq.2) of the failed channel and the second nulled column corresponds to an integrator state (see eq.3). The integrator state $\int \Delta\delta_e \, dt$ is deleted for either a stabilizer failure or an elevator failure, and the integrator state $\int \Delta\delta_{sp} \, dt$ is deleted for a spoiler failure. The reasons for eliminating an integrator state are (1) to delete an obviously bad feedback measurement in the case of a δ_e or a δ_{sp} failure, (2) to allow the elevator freedom to search for a new trim in the case of a δ_s failure and (3) to maintain an equal number of integrators and controls in order to maintain a unique solution for the feedforward control gains.

Closed loop eigenvalues and Bode data are shown in the last three columns of Table I for each single failure case. Each case has 13 eigenvalues (as opposed to 15) and three control channels (as opposed to 4). Again the first two complex eigenvalues represent the phugoid and short period respectively. Other eigenvalues have also been lined up with the corresponding eigenvalues from the 4 controls case.

The phugoid is relatively constant for all cases analyzed, whereas the short period shows large variations for each of the three failure cases and, in addition, the damping ratios are reduced considerably for δ_e and δ_{sp} failures. All other closed loop eigenvalues remain relatively constant. Bode data appears satisfactory for all cases analyzed except for a δ_e failure with the δ_s loop open; the phase margin for this case is reduced to only 18 degrees. The smallest gain margin is 7.3 db for the same case, and the smallest phase margin, other than the case pointed out above, is 45 degrees for a δ_s failure with the δ_e loop open. Open loop eigenvalues (not shown) for the 4 controls case and for each failure case, under conditions of each control loop opened individually, are all stable except for the case of δ_s failure with the δ_e loop open. There is a positive real eigenvalue at S =0.1 for this case.

Closed loop eigenvalues and Bode data have also been calculated for the non-reconfigured control law (no feedback gains altered) with control element failures. The closed loop eigenvalues for each non-reconfigured failure case are identical to the open loop eigenvalues calculated for the corresponding Bode plot in figure 1, where each control channel is opened separately. For the case of a failed δ_e, ,there is a stable but very low damped phugoid mode pole (ζ = 0.025, ω = 0.99 r/s). The Bode gain margin for this failure case is only 0.78 db with the δ_s loop open and is -3.5 db with the δ_{sp} loop open while the phase margin is only 2.3 degrees with the δ_s loop open. This analysis, along with simulation results shown in the following section, illustrate that the reconfigured feedback control law provide the best results.

NONLINEAR SIMULATION

The incremental control law form that combines both the feedback and feedforward gains as described in equations (A28) to (A33) was evaluated in a 6 degree of freedom nonlinear simulation to evaluate the design example cases (4 controls case and failure cases) described in the previous section of this paper. Since the design is only for the longitudinal control channel, an existing autopilot was used to regulate lateral-directional perturbations. The evaluation included both CGT with command changes in altitude rate $\dot{h}$ ($-\dot{Z}$) and airspeed V_a (see equations B1 and B2) and windshear and turbulence penetration capabilities.

CGT Evaluation

The CGT evaluation included separate deceleration and acceleration commands $\ddot{h}_m$ and $\dot{V}_{a,m}$ separated by constant $\dot{h}_m$ and $V_{a,m}$ commands. The four command changes are (1) $\ddot{h}_m$ equal to 2.5 ft/s/s during the 5 to 9 second time period, (2) $\ddot{h}_m$ equal to -2.5 ft/s/s during the 30 to 34 second time period, (3) $\dot{V}_{a,m}$ equal to -5 ft/s/s during the 55 to 60 second time period and (4) $\dot{V}_{a,m}$ equal to 5 ft/s/s during the 80 to 85 seond time period.

Simulation plots for the CGT 4 controls baseline design are shown in figure 2. Both altitude errors (Δh) and airspeed errors (ΔV_a), defined as the difference between the actual output and the commanded output, go to zero during the steady-state condition, demonstrating the type 1 control properties. Pitch attitude θ settles at a new trim value. Two of the controls, δ_e and δ_{sp} return to their trim states during the steady-state time periods, forcing δ_{th} and δ_s to new trim states.

Individual control failures on control elements δ_s, δ_e, and δ_{sp} have been investigated for CGT evaluation. Figure 3 shows results for a non-reconfigured control law with a δ_e failure at 10 degrees (trailing edge down). The low damped phugoid mode oscillation (0.99 r/s) is initially excited by the δ_e step during failure. The same failure case for the reconfigured control law is shown in figure 4. After the initial transient response dies out, the command following capabilities are very similar to those shown in figure 2, with steady state errors Δh and ΔV_a going to zero. The stabilizer settles at a new trim value (-8 deg) to compensate for the δ_e failure. Figure 5 illustrates a CGT evaluation for a δ_s failure at neutral. The integrator on the δ_e control is eliminated, allowing δ_e to settle at a new trim value.

Control Authority To Overcome Stabilizer Failure

A separate test was made to determine the control authority of δ_e under conditions of δ_s failures other than at trim (-4.8 degrees) and with no external disturbances. The elevator command is position limited and rate limited and rate to +/- 10 degrees and +/- 10 degrees/second respectively. Simulation results show that δ_e can overcome moments produced by a δ_s failure only over the range from -1 to -8 degrees. Failures of δ_s outside this range cause δ_e saturation.

Windshear and Turbulence Penetration

The 4 controls design and failure case examples were evaluated for a three degree glideslope approach and landing under the condition of severe windshear and turbulence and with measurement noise characteristic of the sensors on the existing airplane. A Stanford Research Institute (SRI) data package available at Langley Research Center contains a reconstruction of the high severity windshear during the 1975 Eastern Airline crash at John F. Kennedy International Airport, with rms gust intensities up to 13 ft/second. A time simulation of the horizontal and vertical wind components are presented in figure 6; the top curves represent the windshear and the bottom curves represent windshear with turbulence. The time scale changes slightly in the simulation cases to be described due to variations in groundspeed V_g during each run.

Figures 7 and 8 contain simulation results for the 4 controls design, with one small but significant difference between them. Figure 7 shows results for the output $\Delta\underline{y}$ defined in equation (4) whereas results shown in figure 8 are for the case where the feedback gains on ΔV_a are divided in a linearly weighted manner between ΔV_a and ΔV_g. The modified incremental equation for the first component $y_k(1)$ of equation (A28) becomes

$$y_k(1) = (1 - c) V_{a,k} + c V_{g,k} \qquad (5)$$

where the coefficient c is calculated as

$$c = \frac{V_{a,m} - V_g}{50}; \quad 0 \leq c \leq 1 \qquad (6)$$

This modification does not alter the validity of the design analyses since the total velocity feedback gains remain unchanged, but the modification does put a lower limit on the allowable groundspeed. In most cases, V_a will have the larger component of feedback gain, and for the case of a tailwind, all of the feedback gain is applied to regulation of V_a. The limit of 50 ft/s is selected to prevent stall in case of a sudden wind change from headwind to tailwind.

Comparison of the plots for states V_a, Θ and α and controls δ_{th} and δ_s best illustrate the benefits of this modification. In figure 7, V_a shows tight regulation through the peak headwind of approximately 60 ft/s at 75 seconds. At that time there is a sudden decrease in V_a due to the decreased headwind and increased downdraft, resulting in a corresponding increase in δ_{th} at the maximum rate (10 deg/s) with position saturation (60 deg) shortly thereafter. The airplane also has a large increase in Θ with a corresponding control correction in δ_s. Good regulation in Δh is maintained during the run.

In contrast, figure 8 shows that V_a is allowed to increase during the large headwind, with the corresponding decrease being much smaller than the previous case. In addition, V_a never decreases very much below the commanded value, δ_{th} does not reach saturation, Θ remains relatively low during the severe time period, and α remains relatively constant throughout the entire approach and landing. The total run time is approximately 10 seconds shorter due to better regulation of V_g.

Flare occurs during the final 42 feet (approximately last 5 seconds) of each run. The objective is to land with a small pitch-up attitude (Θ = 1 to 2 deg) and a low rate of descent ($\dot{h}$ = -1 to -3 ft/s). The CGT commanded a deceleration of 3 ft/s/s simultaneously with the reduced rate of descent; both of these commands cause Θ to go to an increased trim value.

Several off-nominl cases have been run for the 4 controls case: these include variation of glideslope, airspeed, airplane weight and CG location. Simulation results show essentially the same regulation as those of figure 7. The airspeed/groundspeed feedback gain tradeoff was not simulated for the off-nominal cases.

Failure Cases

Simulation results for the following failure cases are to be compared to the modified configuration as shown in figure 8. Failure cases have been simulated with single control element failures at either the neutral (trim) position or at the maximum allowable excursion. Neutral postions are (1) -4.8 degrees for δ_s, (2) zero degrees for δ_e and (3) 8 degrees for δ_{sp}. All failures to be shown occur at time 30 seconds with FDI assumed to be operational as described in the section on the design example. Simulation results for failures at neutral are all similar to those shown in figure 8. An example case for a δ_{sp} failure at 8 degrees is shown in figure 9. As expected, Δh regulation is slightly degraded due to the loss of the direct lift control. Larger control excursions can be seen in δ_e, although the control remains well within the linear region, and δ_s appears biased at a slightly lower trailing edge up position.

Safe flight can be maintained with either control element failures δ_e or δ_{sp} at their maximum excursions; δ_e command is position limited to +/- 10 degrees and δ_{sp} command is limited between 0 and 16 degrees. An example case is shown in figure 10 for a δ_e failure at 10 degrees (trailing edge down). The stabilizer is forced to a higher trailing edge up trim value, and is also seen to be more oscillatory, due to the low damped short period. Both $\dot{h}$,Θ and q have increased oscillations, although for the most part results are similar to those of the 4 controls design.

Previous analysis has indicated that, for the case without external disturbances, safe flight can be maintained if δ_s failures are limited between the range of -1 to -8 degrees (trailing edge up). This range is reduced considerably when external disturbances, representative of the Kennedy windshear and turbulence, are applied. Good control is maintaned with a δ_s failure at -2 degrees (figure 11), but a δ_s failure at -5.5 degrees (figure 12) shows marginal safety. In both cases, δ_e activity is increased to take over for the δ_s failure, but for the case in figure 12, δ_e saturates

trailing edge down during the time period of the two major downbursts (figure 6). The critical portion is during the decreasing downburst period, when altitude Δh increases and the forces and moments produces by δ_e cannot overcome those produced by the decreasing downburst plus those due to the δ_s failure. In addition, δ_{th} saturates during the time period of headwind to tailwind change. Figure 13 shows the airplane stalling with a δ_s failure of -6.5 degrees.

Three Controls Design

A new design was made to get an optimized set of feedback gains using only three controls (δ_{th}, δ_e, δ_{sp}), leaving out the stabilizer. This new level of reconfiguration was done to determine if the range for overcoming a δ_s failure can be widened. A set of nominal weightings was put into the output feedback program, and the design was evaluated without readjustment. Nonlinear simulations were made with δ_{sp} commanded to trim values other than the 8 degrees used for design, in order to add additional forces and moments to help overcome those produced by δ_s. Figure 14 shows results for the 3 controls design with a δ_s failure at -1.0 degree and δ_{sp} commanded to 12 degrees after FDI. Figure 15 shows results for a δ_s failure at -6.5 degrees with δ_{sp} commanded full down (0 degrees) after FDI. Although this latter case is again marginally safe, the approach shows that improvement can be obtained by a redesign and the judicious use of control moments to counteract those resulting from the failure.

CONCLUSIONS

The objective of this paper is to describe a control law design that allows the airplane to recover to a safe condition for landing in the presence of a control element failure even though performance may be degraded. All sensors and computers are assumed to be fully operational, as well as failure detection and identification algorithms that supply needed information to the control logic. A PIF discrete control structure formulation is combined with a discrete output feedback design program to calculate the optimal feedback gains. Open loop feedforward gains are included at the output of a command generator tracker. All flight equations are implemented in incremental form using total measurements.

The longtudinal axis of a B-737 airplane is used for the design example. The PIF model includes 7 plant states, 4 control position-command states, 4 integrator states to give type 1 properties to commanded outputs, and 4 control rate-command states to accommodate the computational delay and provide additional filtering.

Closed loop eigenvalue analysis and Bode analysis have been made for a nominal 4 controls baseline design and three single failure cases. The non-reconfigured control law is unsatisfactory for the δ_e failure case. The closed loop phugoid mode is extremely low damped, and the Bode gain and phase margins are very low. The reconfigured control law used a subset of the output feedback gains. The phugoid mode is relatively constant for all failure cases, whereas the short period mode shows large closed loop eigenvalue variations and has low damping ratios for δ_e and δ_{sp} failures. All other closed loop eigenvalues remain relatively constant. The lowest Bode gain margin is 7.3 db for a δ_e failure with the δ_s loop open. The phase margin is at least 45 degrees for all cases except for the case just

mentioned, which has a phase margin of only 18 degrees. All failure cases remain open loop statically stable except for the δ_s failure case with one real positive eigenvalue at S=0.1.

All designs are verified using a 6 degree of freedom nonlinear simulation. The command generator tracking evaluation demonstrated type one properties for all four integrator states, whereas non-integrated states are forced to new trim vaues. Investigation of failure cases at neutral position show similar results.

All designs are tested under the conditions of the high severity Kennedy windshear reconstruction and thunderstorm type turbulence. A key feature is the allocation of velocity feedback gains between airspeed and groundspeed, which puts a lower limit on the allowable groundspeed to help prevent stall. Incorporation of this feature results in a reduced airspeed drop during a loss of headwind, nonsaturation of δ_{th}, pitch attitude remaining under 12 degrees during the severe downdraft and reduced headwind/increased tailwind portion of flight, and a relatively constant aerodynamic angle of attack. The 4 controls design shows that the airplane lands with a low rate of descent, as commanded, and with a small pitch up attitude. Reducing airspeed and rate of descent forced the pitch attitude to the new trim condition.

During simulation, failures occurred 30 seconds into the run, with the assumption that FDI is fully operational. Simulation of control element failures at neutral show results very similar to the 4 controls design. Safe flight can be maintained with either the elevator or spoilers failed at any hard over position.

On the B-737, the stabilizer must fail within a limited range to overcome the control moments. Without extenal disturbances, the elevator can overcome these moments if δ_s remains in the range from -1 to -8 degrees (trailing edge up). With the addition of the Kennedy windshear and turbulence, the δ_s failure range for the 4 controls design is reduced to the region of -2 to -5.5 degrees. A redesign, restructuring the three remaining operational controls and a set of nominal weightings without readjustment, shows that the δ_s range can be widened (-1 degree to -6.5 degrees). During simulation for the latter case, the spoilers are commanded to new steady state values to help produce moments compensating those produced by δ_s.

APPENDIX A

MATHEMATICAL FORMULATION

A PIF/CGT formulation has been integrated with a discrete output feedback design program. Special features of the PIF structure have been described in the paper. This appendix contains the mathematical description of the PIF structure, output feedback equations, command generator equations and the equations implementd for simulated flight.

PIF Formulation

The continuous time design model using the PIF form is given by

$$\dot{\Delta\bar{x}} = \bar{A}\ \Delta\bar{x} + \bar{B}\ \Delta v + \bar{E}\ \ \Delta\bar{w} \tag{A1}$$

$$\Delta\bar{y} = \bar{H}\ \Delta\bar{x} + \bar{n} \tag{A2}$$

$$\Delta\bar{x} = \left[\ \Delta x^T,\ \Delta u^T,\ \Delta z^T\right]^T \tag{A3}$$

$$\Delta w = \left[\ \Delta w^T,\ n_z{}^T\ \right]^T \tag{A4}$$

$$\bar{A} = \begin{bmatrix} A & B & 0 \\ 0 & 0 & 0 \\ H_z & D_z & 0 \end{bmatrix} \tag{A5}$$

$$\bar{B} \begin{bmatrix} 0 \\ I \\ 0 \end{bmatrix} \tag{A6}$$

$$\bar{E} = \begin{bmatrix} E & 0 \\ 0 & 0 \\ 0 & I \end{bmatrix} \tag{A7}$$

where Δx is the plant state, Δu is the control position-command state, Δz is the integrator state, Δv is the control rate-command, Δw is the wind gust, n_z is the noise on the integrator state, $\Delta\bar{y}$ is the output vector, $\bar{n}$ is the output noise, $\underline{A}$ and B are the plant state and control matrices, E is the wind gust matrix, $\bar{H}$ is the output matrix, H_z and D_z are transmission matrixes for the plant and control states to be integrated, and I is an identify matrix.

The discrete form of equations (A1) and (A2) is obtained using the ORACLES computer program (ref. 19) as

$$\Delta\bar{x}_{k+1} = \bar{F}\ \Delta\bar{x}_k + \bar{G}\ \Delta v_k + \bar{G}_w\ \Delta\bar{w}_k \tag{A8}$$

$$\Delta\bar{y}_k = \bar{H}\ \Delta\bar{x}_k + \bar{n}_k \tag{A9}$$

where $\bar{F}$, $\bar{G}$, and $\bar{G}_w$ are the discrete matrices corresponding to $\bar{A}$, $\bar{B}$, and $\bar{E}$ respectively. Approximations (ref. 8) are made to $\bar{F}$ and $\bar{G}$ in order to implement both a zero-order hold for the control rate-commands (as compared to a triangular data hold) and an Euler discrete integration. The final form for both $\bar{F}$ and $\bar{G}$ become

$$\bar{F} = \begin{bmatrix} F & G & 0 \\ 0 & I & 0 \\ \Delta T.\ H_z & \Delta T.\ D_z & I \end{bmatrix} \tag{A10}$$

$$\bar{G} = \begin{bmatrix} 0 \\ \Delta T.I \\ 0 \end{bmatrix} \tag{A11}$$

where ΔT is the discrete sampling period.

Output Feedback Equations

A stochastic discrete optimal output feedback design program (ref. 17) has been used to compute feedback gains for the selected outputs of equation (A9). Starting with the continuous time cost function J given by

$$J = E\left(\int_0^\infty \left[\Delta\bar{x}^T \bar{Q} \Delta\bar{x} + \Delta v^T R_v \Delta v \right] dt \right) \tag{A12}$$

where E is the expected value and where $\bar{Q}$ is a diagnonal state weighting matrix with components given by

$$\bar{Q} = \text{diag}\left[Q_x, R_u, Q_z \right] \tag{A13}$$

with Q_x the weighting for the Δx plant state, R_u the weighting for the Δu control position-command state, and Q_z the weighting for the Δz integrator state. The weighting for the control rate-command state is represented by the diagonal R_v. All weightings, described in the next section, are inserted into equation (A12).

The equivalent discrete performance index, which is required in reference 17, is defined as

$$J = \lim_{N\to\infty} \frac{1}{N} E \left(\sum_{k=-1}^{N} \Delta\bar{x}_k^T \hat{Q} \Delta\bar{x}_k + 2\Delta\bar{x}_k^T \hat{M} \Delta v_k + \Delta v_k^T \hat{R} \Delta v_k \right) \tag{A14}$$

where $\hat{Q}$, $\hat{M}$, $\hat{R}$ are the discrete weighting matrices corresponding to $\bar{Q}$ and R_v as calculated using reference 19 for sampling period ΔT.

The optimal feedback gains K are directly related to the output measurement as

$$\Delta v_k = K \Delta\bar{y}_k \tag{A15}$$

with the corresponding closed loop transition matrix F_{cl} as

$$F_{cl} = \bar{F} + \bar{G} K \bar{H} \tag{A16}$$

The output feedback formulation also includes both plant process noise and measurement noise. Terms included in the plant process noise are randomly distributed initial condition errors, control input random pseudonoise, random wind gust disturbances, and integrator noise. The total plant process noise covariance $\bar{\bar{W}}$ is calculated as

$$\bar{\bar{W}} = \bar{F}\ \bar{X}_o\ \bar{F}^T + \int_0^{\Delta T} [\exp(\bar{A}\,t)]\,[\bar{B}\ V_o\ \bar{B}^T + \bar{E}\ W_o\ \bar{E}^T]\,[\exp(\bar{A}^T t)]\,dt \quad \text{(A17)}$$

$$E(\Delta\bar{x}_o) = 0 \quad \text{(A18a)}$$

$$E(\Delta\bar{x}_o\ \Delta\bar{x}_o^T) = \bar{X}_o\ \delta_{t\tau} \quad \text{(A18b)}$$

$$E(\Delta v) = 0 \quad \text{(A19a)}$$

$$E(\Delta v\ \Delta v^T) = V_o\ \delta_{t\tau} \quad \text{(A19b)}$$

$$E(\Delta\bar{w}) = 0 \quad \text{(A20a)}$$

$$E(\Delta\bar{w}\ \Delta\bar{w})^T = W_o\ \delta_{t\tau} \quad \text{(A20b)}$$

where $\bar{X}_o$ is the initial condition covariance, V_o is the control input pseudonoise covariance, W_o is the wind gust and integrator noise covariance, t is a dummy time variable, and $\delta_{t\tau}$ is the Kronecker delta. The integral term in equation (A17) is transformed to discrete formulation using ORACLS (reference 19). The measurement noise covariance $\bar{V}$ is calculated in a similar manner as

$$E(\bar{n}) = 0 \quad \text{(A21a)}$$

$$E(\bar{n}\,\bar{n}^T) = \bar{V}\ \delta_{t\tau} \quad \text{(A21b)}$$

Command Generator Tracking (CGT)

The objective of CGT is to cause selected outputs Δy of the airplane to optimally track the output Δy_m of a linearized command model using feedforward control theory. Using symbology defined previously, the open loop plant model is:

$$\Delta x_{k+1} = F\,\Delta x_k + G\,\Delta u_k \quad \text{(A22)}$$

$$\Delta y_k = H_z \Delta x_k + D_z\,\Delta u_k \quad \text{(A23)}$$

and the linearized command model is

$$\Delta x_{m,k+1} = F_m \Delta x_{m,k} + G_m \Delta u_{m,k+1} \quad \text{(A24)}$$

$$\Delta y_{m,k} = H_m \Delta x_{m,k} + D_m \Delta u_{m,k+1} \quad \text{(A25)}$$

The reason for using an advanced time step on the control command Δu_m is to resolve a mathematical contradiction due to the discontinuity when Δu_m changes. A more complete description is presented in reference 8 and chapter 4.10 of reference 9. Feedforwaed gains relate the model state (Δx_m) and Δu_m to an ideal star trajectory Δx^*, Δu^* as

$$\begin{bmatrix} \Delta x_k^* \\ \Delta u_k^* \end{bmatrix} = \begin{bmatrix} A11 & A12 \\ A21 & A22 \end{bmatrix} \begin{bmatrix} \Delta x_{m,k} \\ \Delta u_{m,k+1} \end{bmatrix} \quad \text{(A26)}$$

where each Aij represents a constant feedforward gain matrix. The solution for the feedforward gains involve the solving of equation A27 as

$$\begin{bmatrix} A11 & A12 \\ A21 & A22 \end{bmatrix} = \begin{bmatrix} (F-I) & G \\ H_z & D_z \end{bmatrix}^{-1} \begin{bmatrix} A11\,(F_m - I) & A11\,G_m \\ H_m & D_m \end{bmatrix} \quad \text{(A27)}$$

The derivation of equation(A27) and a method to solve it are presented in reference 11.

Flight Equations

The CGT model is integrated into the feedback design by letting the pertubation model (eq. A8) represent the error between the plant perturbation states and controls and the star trajectory perturbation states and controls. Using an incremental control law form and rigorously substituting total quantities into the perturbation model similar to reference 8 (full state feedback as opposed to output feedback for this paper), the flight equations become

$$e_k = y_k - \bar{H}_x \; A11 \; x_{m,k} \quad \text{(A28)}$$

$$v_k = (I + \Delta T\, K\, \bar{H}_u)\, v_{k-1} + K(e_k - e_{k-1}) + \Delta T\, K\, \bar{H}_z\, (H_z\, Y_{x,k-1} + D_z\, u_{k-1} - y_{m,k-1}) + E1(u_{m,k+1} - u_{m,k}) \quad \text{(A29)}$$

where

$$u_{k+1} = u_k + \Delta T\, v_k \tag{A30}$$

$$\bar{H} = [\bar{H}_x \quad \bar{H}_u \quad \bar{H}_z] \tag{A31}$$

$$E1 = -K[\bar{H}_x\ A12 + \bar{H}_u\ A22 + \bar{H}_z\ P_A] \tag{A32}$$

$$P_A = -P_{zz}^{-1}\,[\,P_{xz}^T\ A12 + P_{uz}^T\ A22\,] \tag{A33}$$

and P_{xz}^T, P_{uz}^T, and P_{zz} represent the last z rows of the optimal output feedback solution matrix of equation of A14.

APPENDIX B

FEEDBACK WEIGHTING APPROACH WITH FEEDBACK AND FEEDFORWARD GAINS

Feedback Gains

The weighting approach used for $\bar{Q}$ and R_v (equation A12) is to calculate the inverse square of the maximum permissible deviations (ΔMax) from the nominal state and control time histories. Table II shows the following columns for each design variable (Δx, Δu, Δz, Δv, Δw, $\Delta \bar{y}$) : (1) ΔMax, (2) initial condition uncertainties and (3) random noise. All of this data is used to calculate the weightings in Table III for the output feedback design program. Only two variables are shown for $\Delta \bar{y}$ in Table II since three of the Δx states and all of the Δu and Δz states, which are included in the $\Delta \bar{y}$ vector, are given above in the random noise column. Output feedback gains K (see eq. A15) for the 13 outputs $\Delta \bar{y}$ going to the 4 control rate-commands Δv are shown in Table IV.

Feedforward Gains

The integrator states defined in equation (3) for the feedback design are chosen to be the same as the outputs Δy_m of the linearized command generator model. The specific model used has the form corresponding to equations (A24) and (A25) as:

$$\Delta Z_{m,k+1} = \Delta Z_{m,k} + [\Delta T \quad 0 \quad 0 \quad 0] \begin{bmatrix} \Delta \dot{Z}_m \\ \Delta V_{a,m} \\ \Delta \delta_{e,m} \\ \Delta \delta_{sp,m} \end{bmatrix}_{k+1} \tag{B1}$$

$$\begin{bmatrix} \Delta Z_m \\ \Delta V_{a,m} \\ \Delta \delta_{e,m} \\ \Delta_{sp,m} \end{bmatrix}_k = \begin{bmatrix} 1 \\ 0 \\ 0 \\ 0 \end{bmatrix} \Delta Z_{m,k} + \begin{bmatrix} 0 & 0 & 0 & 0 \\ 0 & 1 & 0 & 0 \\ 0 & 0 & 1 & 0 \\ 0 & 0 & 0 & 1 \end{bmatrix} \begin{bmatrix} \dot{\Delta Z}_m \\ \Delta V_{a,m} \\ \Delta \delta_{e,m} \\ \Delta \delta_{sp,m} \end{bmatrix}_{k+1} \quad \text{(B2)}$$

Using equation (A27), the feedforward gains become

$$A11 = \begin{bmatrix} 0. \\ 0. \\ 0. \\ 0. \\ 1. \\ 0. \\ 0. \end{bmatrix} \quad \text{(B3)}$$

$$A12 = \begin{bmatrix} -2.65E-3 & 1.03E+0 & 4.71E-6 & -1.17E-1 \\ 3.64E-2 & 4.42E-1 & -6.47E-5 & 1.61E+0 \\ 0. & 0. & 0. & 0. \\ -4.47E-3 & -2.15E-1 & -3.01E-7 & 7.51E-3 \\ 0. & 0. & 0. & 0 \\ -3.25E-1 & 4.58E-2 & 1.14E-5 & 3.85E-1 \\ -3.97E-2 & 4.09E-2 & -3.19E-1 & 1.09E-1 \end{bmatrix} \quad \text{(B4)}$$

$$A21 = \begin{bmatrix} 0. \\ 0. \\ 0. \\ 0. \end{bmatrix} \quad \text{(B5)}$$

$$A22 = \begin{bmatrix} -6.51E-1 & 9.16E-2 & -2.28E-5 & 7.70E-1 \\ -5.96E-2 & 6.13E-2 & -4.79E-1 & 1.64E-1 \\ 0. & 0. & 1.00 & 0. \\ 0. & 0. & 0. & 1.00 \end{bmatrix} \quad \text{(B6)}$$

REFERENCES

(1)Rynaski, Edmund: Experimental Experience at Calspan. Workshop On Restructurable Controls, pp. 99-114, NASA CP-2277, September 1982.

(2) Howell, W. E., Bundick, W. T., Hueschen, R. M., Ostroff, A. J.: Restructurable Controls for Aircraft. AIAA Guidance and Control Conference, Gatlinburg, Tennessee, August 15-17, 1983.

(3) Howell, W. E., et al: Workshop on Restructurable Controls. NASA CP-2277, September 1982.

(4) Athans, Michael: On Restructurable Control System Theory. Workshop on Restructurable Controls, pp. 9-42, NASA CP-2277, September 1982.

(5) Cunningham, Thomas B.: Robust Configuration for High Reliability and Survivability for Advanced Aircraft. Workshop on Restructurable Controls, pp. 43-79, NASA CP-2277, September 1982.

(6) Potts, David W.: Direct Digital Design Method for Reconfigurable Multivariable Control Laws for the A-7D DIGITAC II AIRCRAFT. Master of Science Thesis, Air Force Institute of Technology, Air University, December 1980.

(7) Dispersed and Reconfigurable Digital Flight Control System, Volume 1. Grumman Aerospace Corporation, AFFDL-TR-79-3125, Bethpage, New York, December 1979.

(8) Broussard, John R.: Design, Implementation and Flight Testing of PIF Autopilots for General Aviation Aircraft. Information and Control Systems Incorporated, NAS1-16303, NASA CR-3709, 1983.

(9) Maybeck, Peter S.: Stochastic Models, Estimation, and Control, Vol. 3. Academic Press, New York, 1982.

(10) Broussard, John R., and O'Brien, M. J.: Feedforward Control to Track the Output of a Forced Model. IEEE Trans. Automatic Control, Vol. 25, August 1980, pp. 851-854.

(11) Berry, Paul W., Broussard, John R., Gully, Sol: Stability and Control Analysis of V/STOL Type B Aircraft. The Analytic Sciences Corporation; March 31, 1979.

(12) Broussard, John R.: Command Generator Tracking - The Discrete Time Case. TIM NO 612-2, The Analytic Sciences Corp., Reading, Massachussetts, March 1978.

(13) Broussard, J.R., Berry, P.W. and Stengel, R.F.: Modern Digital Flight Control Systems Design for VTOL Aircraft. NASA CR-159019, March 1979.

(14) Broussard, J.R., Downing, D.R. and Bryant, W.H.: Design and Flight Testing of a Digital Optimal Control General Aviation Autopilot. Proceedings of the 13th Congress of the International Council of the Aeronautical Sciences/AIAA Aircraft Systems and Technology Conference, Seattle, Washington, August 22-27, 1982.

(15) Broussard, J.R., Bryant, W.H., Downing, D.R.: Design and Flight Testing of a Digital Landing Approach Autopilot. 1983 American Control Conference, San Francisco, California, June 22-24, 1983.

(16) Downing, David R.: Restructurable Controls Problem Definition and Future Research. Workshop on Restructurable Controls, pp. 81-98, NASA CP-2277, September 1982.

(17) Halyo, N. and Broussard, J. R.: A Convergent Algorithm for the Stochastic Infinite-Time Discrete Optimal Output Feedback Problem. Proceedings of the 1981 JACC, Charlottesville, VA, June 1981.

(18) Broussard, J.R., and Halyo, N.: Active Flutter Suppression Using Optimal Output Feedback Digital Controllers, NASA CR-165939, May 1982.

(19) Armstrong, E.S.: ORACLS - A Design System for Linear Multivarible Control. Marcel-Dekher, Inc., New York, 1980.

SYMBOLS

A	plant continuous state matrix
$\bar{A}$	PIF continuous state matrix
A11,A12 A21,A22	feedforward gains
B	plant continous control matrix
$\bar{B}$	PIF continuous control matrix
c	coefficient for airspeed and groundspeed feedback gains
D_m	control observation matrix for command model
D_z	transmission matrix for control integrator states
E	wind gust disturbance matrix
$E(\ )$	expectation operator
$\bar{E}$	PIF disturbance matrix
El	control matrix for incremental flight equations
e	error vector used in incremental flight equations
F	plant discrete state transition matrix
$\bar{F}$	PIF discrete state transition matrix
F_{cl}	discrete closed loop transition matrix
F_m	command model discrete state transition matrix
G	discrete plant control matrix
$\bar{G}$	PIF discrete control matrix
G_M	gain margin
G_m	command model discrete control matrix
$\bar{G}_w$	PIF discrete disturbance matrix
$\bar{H}$	PIF state observation matrix
$\bar{H}_x, \bar{H}_u, \bar{H}_z$	column partitions of $\bar{H}$ corresponding to x,u,z states
H_m	command model state observation matrix

H_z	integrator output observation matrix
h	altitude of airplane, positive up (ft)
$\ddot{h}_m$	command model vertical acceleration (ft/s/s)
I	identity matrix
J	cost function
K	optimal feedback gain matrix
k	sample integer
$\overset{\Lambda}{M}$	PIF discrete cost function cross weighting matrix between states and controls
N	number of samples in discrete performance index
$\bar{n}$	noise on PIF outputs
n_z	noise on integrator outputs
P_A	discrete feedforward matrix
P_M	phase margin
P_{xy}, P_{uz}, P_{zz}	last z rows of output feedback solution matrix corresponding to x, u, and z respectively
$\bar{Q}$	PIF continuous state weighting matrix
$\overset{\Lambda}{Q}$	PIF discrete cost function state weighting matrix
Q_x, Q_z	subset of $\bar{Q}$ relating to x plant states or z integrator states respectively
q	pitch rate (rad/s for equations) (deg/s for plots)
$\overset{\Lambda}{R}$	PIF discrete cost function control weighting matrix
R_u	subset of $\bar{Q}$ for u control states
R_v	PIF continuous control weighting matrix
S	eigenvalue (rad/s)
t	time (sec)
U	body longitudinal axis inertial velocity component, positive forward (ft/s)
u	control position-command state vector

u_m	command model control vector
$\bar{V}$	measurement noise covariance matrix
V_a	airspeed (ft/s)
$\dot{V}_{a,m}$	command model longitudinal acceleration (ft/s/s)
V_g	groundspeed (ft/s)
V_o	control input process noise covariance matrix
v	control rate-command vector
W	body vertical axis inertial velocity component, positive down (ft/s)
$\overset{\Delta}{W}$	total plant process noise discrete covariance matrix
W_o	plant process noise covariance matrix for random wind gust and integrator noise
$\bar{w}$	wind gust and integrator noise vector
$\bar{X}_o$	initial condition error vector
x	plant state vector
$\bar{x}_o$	PIF state vector
$\dot{\bar{x}}$	time derivative of PIF state vector
x_m	command model state vector
$X\delta_s$	stabilizer servo filter state
$X\delta_t$	throttle dynamics filter state
y	plant output measurement vector
y_x	output related to the x plant states
$\bar{y}$	PIF output vector
y_m	command model output vector
Z	negative of h, (ft)
$\dot{Z}$	time derivative of Z, positive down (ft/s)
z	integrator state vector
α	aerodynamic angle of attack (deg)

γ	flight path angle (deg)
Δ	perturbation
ΔT	discrete sampling period (sec)
δ_e	elevator control (deg)
δ_s	stabilizer control (deg)
δ_{sp}	spoiler control (deg)
δ_{th}	throttle control (deg)
$\delta_{t\tau}$	Kronecker delta
ζ	damping ratio
θ	pitch attitude (rad for equations) (deg for plots)
ω	radian frequency (rad/s)

Subscripts

m	command model
z	integrator terms

Superscripts

T	transpose
*	ideal star trajectory

Table 1 - Eigenvalue and Bode Data

OPEN LOOP

Plant S	ζ
-0.019±.17j	.11
-0.59 ±1.1j	.47
-1.5	
-2.0	

CLOSED LOOP

4 Controls S	ζ
-.38±.58j	.55
-1.47±2.3j	.54
- .23±.19j	.76
- .60±.16j	.97
- .76	
-1.1	
-1.8	
-2.4±2.3j	.73
-2.7	
-7.7	

δs Failed S	ζ
-.31±.71j	.40
-1.6±1.0j	.85
-.22±.20j	.75
-.67±.12j	.98
-1.5	
-1.9	
-2.9±2.4j	.77
-3.1	

δe Failed S	ζ
-.45±.64j	.58
-.38±1.3j	.27
-.23±.19j	.76
-.87±.16j	.98
-.70	
-2.5±2.2j	.75
-2.6	
-7.3	

δsp Failed S	ζ
-.26±.52j	.45
-.78±2.7j	.28
-.21±.20j	.74
-.50±.13j	.97
-.76	
-1.5±.76j	.90
-2.6	
-7.6	

BODE DATA

	w rad/s	Pm deg	Gm db	w rad/s	Pm deg	Gm db	w rad/s	Pm deg	Gm db	w rad/s	Pm deg	Gm db
δ_{th} open	.34	49		.33	48		.33	49		.33	47	
	1.6		-18	1.6		-18	1.6		-16	1.7		-20
δ_s open	.80	82					.21		38			
	3.8		-14				.63		8.5	.82	101	
δ_e open	.48	-94		.56		10	1.3	18		3.4		-9.8
	2.2	57		1.5	45		2.4		-7.3			
	6.9		-15	6.9	165					.38	-105	
δ_{sp} open	.68	-140		.66	-108		.64	-135		2.7	35	
	1.1	141		1.2	125		.96	127		6.1		-13
	7.9		-19	8.0		-19	1.6	-159				
							2.2	103				
							7.6		-18			

Table II. - Data for Selection of State and Control Weightings, Process Noise Covariance, Measurement Noise Covariance

	Variable	Unit	ΔMax	Initial Cond	Random Noise
Δx	Δu	ft/s	30.	10.	
	Δw	ft/s	3.	1.	
	q	r/s	.1	.01	.00035
	$\Delta\theta$	r	.2	.03	.004
	ΔZ	ft	20.	20.	3.
	$\Delta\chi\delta_t$	deg/r/s	4.	2.	
	$\Delta\chi\delta_s$	deg/r/s	3.	1.	
Δu	$\Delta\delta_{th}$	deg	4.	4.	.01
	$\Delta\delta_s$	deg	5.	1.7	.01
	$\Delta\delta_e$	deg	10.	2.	.01
	$\Delta\delta_{sp}$	deg	8.	2.	.01
Δz	$\int\Delta Z\,dt$	ft-s	7.	0.	.07
	$\int\Delta V_a\,dt$	ft	10.	0.	.1
	$\int\Delta\delta_e\,dt$	deg-s	7.	0.	.01
	$\int\Delta\delta_{sp}\,dt$	deg-s	2.	0.	.01
Δv	$\Delta\dot{\delta}_{th}$	deg/s	4.		.1
	$\Delta\dot{\delta}_s$	deg/s	10.		.1
	$\Delta\dot{\delta}_e$	deg/s	10.		.1
	$\Delta\dot{\delta}_{sp}$	deg/s	20.		.2
Δw	Δu_w	ft/s			10.
	Δw_w	ft/s			7.5
$\Delta\bar{y}$	ΔV_a	ft/s			2.5
	$\Delta\dot{Z}$	ft/s			1.0

Table III. - Weighting for Output Feedback Design Program

$\bar{Q}$	R_v	$\bar{X}_o$	V_o	W_o	$\bar{V}$
1.1E-3	6.3E-2	1.0E+2	1.0E-2	1.0E+2	6.3
1.1E-1	1.0E-2	1.0	1.0E-2	5.6E+1	1.0
1.0E+2	1.0E-2	1.6E-3	1.0E-2	4.9E-3	1.2E-7
2.5E+1	2.5E-3	2.5E-3	4.0E-2	1.0E-2	1.6E-5
2.5E-3		4.0E+2		1.0E-4	9.0
6.3E-2		4.0		1.0E-4	1.0E-4
1.1E-1		1.0			1.0E-4
6.3E-2		1.6E+1			1.0E-4
4.0E-2		2.9			1.0E-4
1.0E-2		4.0			4.9E-3
1.6E-2		4.0			1.0E-2
2.0E-2		0.			1.0E-4
1.0E-2		0.			1.0E-4
2.0E-2		0.			
2.5E-1		0.			

Table IV - Feedback Gains (K)

$\Delta\bar{y}$	$\Delta v(1)$	$\Delta v(2)$	$\Delta v(3)$	$\Delta v(4)$
ΔV_a	- 2.33	+ .459	+ .948	+ .463
$\Delta\dot{Z}$	+ .378	- 2.00	- 3.69	- 1.55
q	-18.0	+270.	+400.	-292.
$\Delta\theta$	-23.4	+394.	+560.	-482.
ΔZ	+ .416	- 1.72	- 3.44	- 1.16
$\Delta u(1)$	- 1.69	+ .517	+ .516	- .030
$\Delta u(2)$	- .138	- 4.71	- .663	- .349
$\Delta u(3)$	+ .0991	- 1.12	- 4.51	+ 1.79
$\Delta u(4)$	- .154	+ .600	+ .895	- 6.03
$\Delta z(1)$	+ .0460	- .393	- .952	- .647
$\Delta z(2)$	- .354	- .119	- .112	+ .283
$\Delta z(3)$	+ .0005	+ .247	- 1.97	+ .871
$\Delta z(4)$	- .557	+ 1.71	+ 2.12	- 7.26

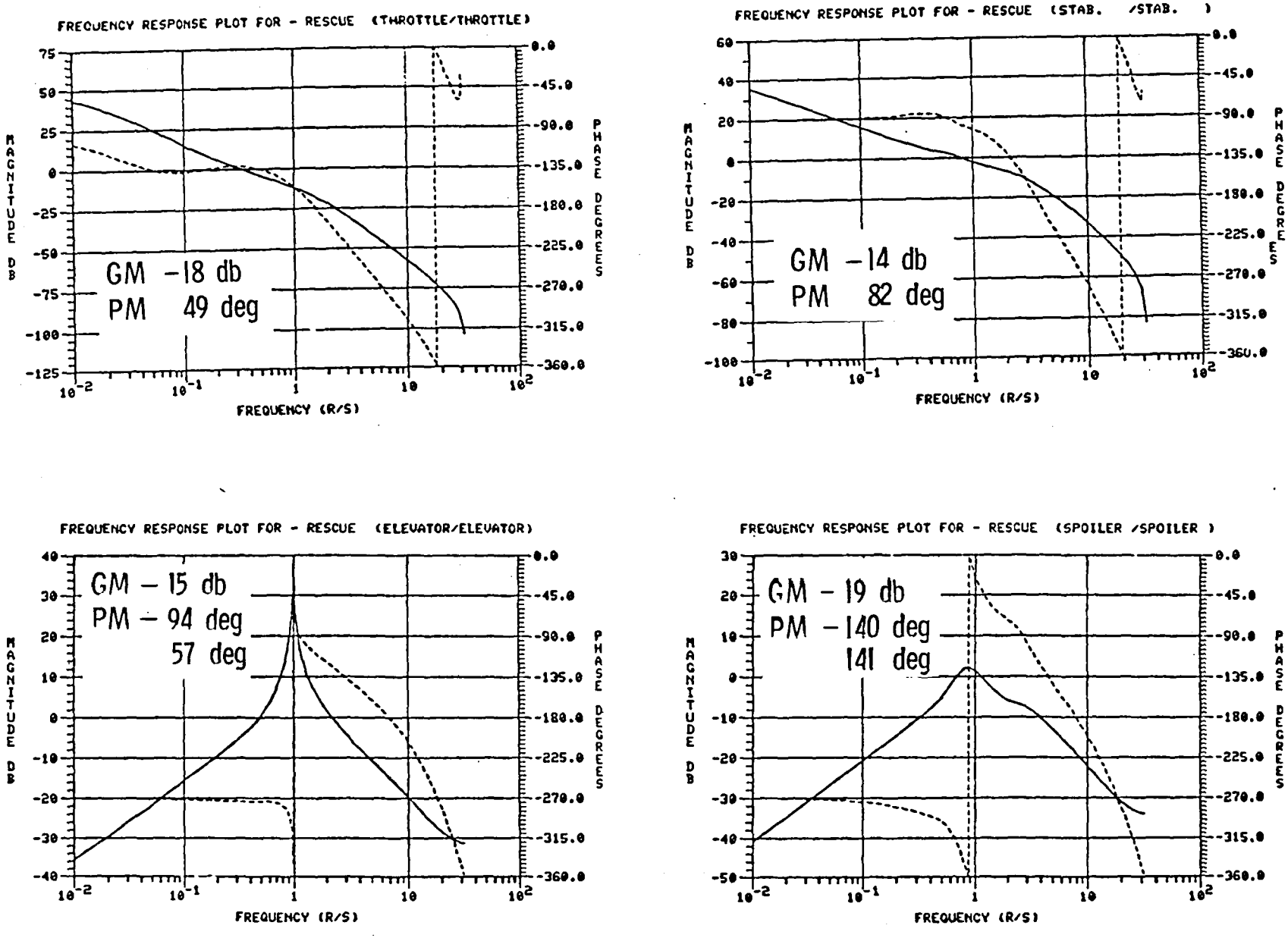

Figure 1 - Bode plots for 4 controls design.

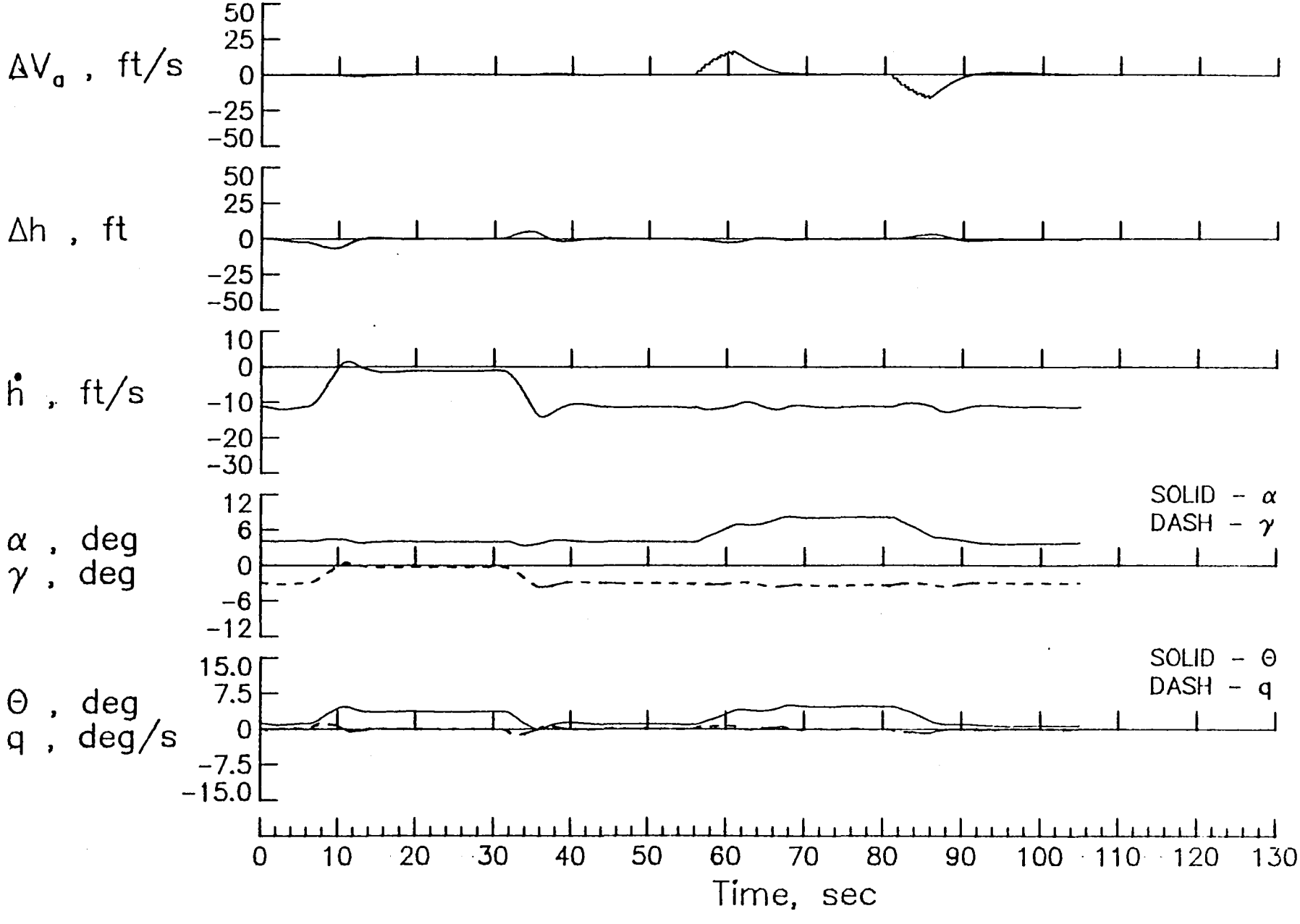

Figure 2 - CGT, 4 controls baseline design.

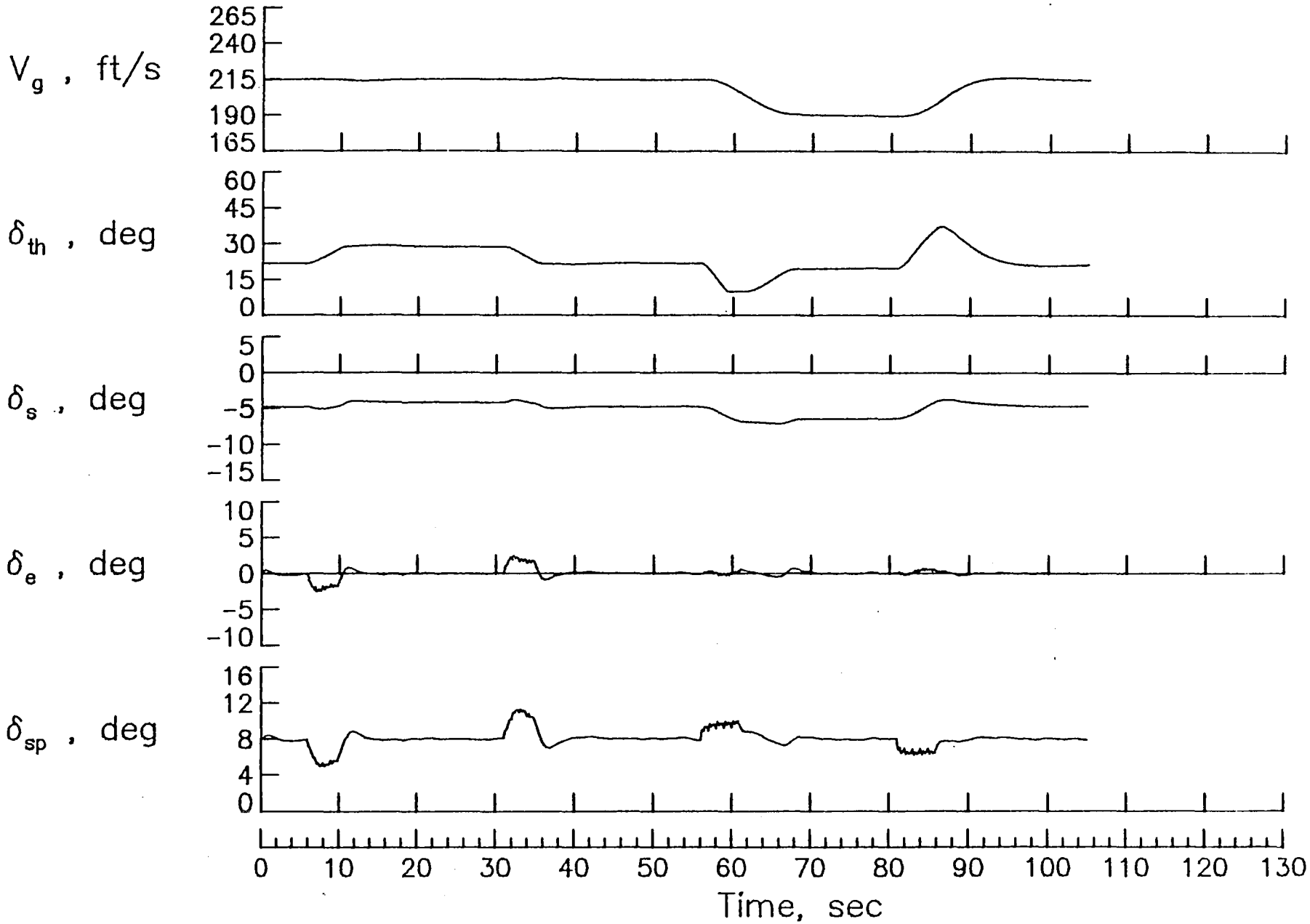

Figure 2 - concluded.

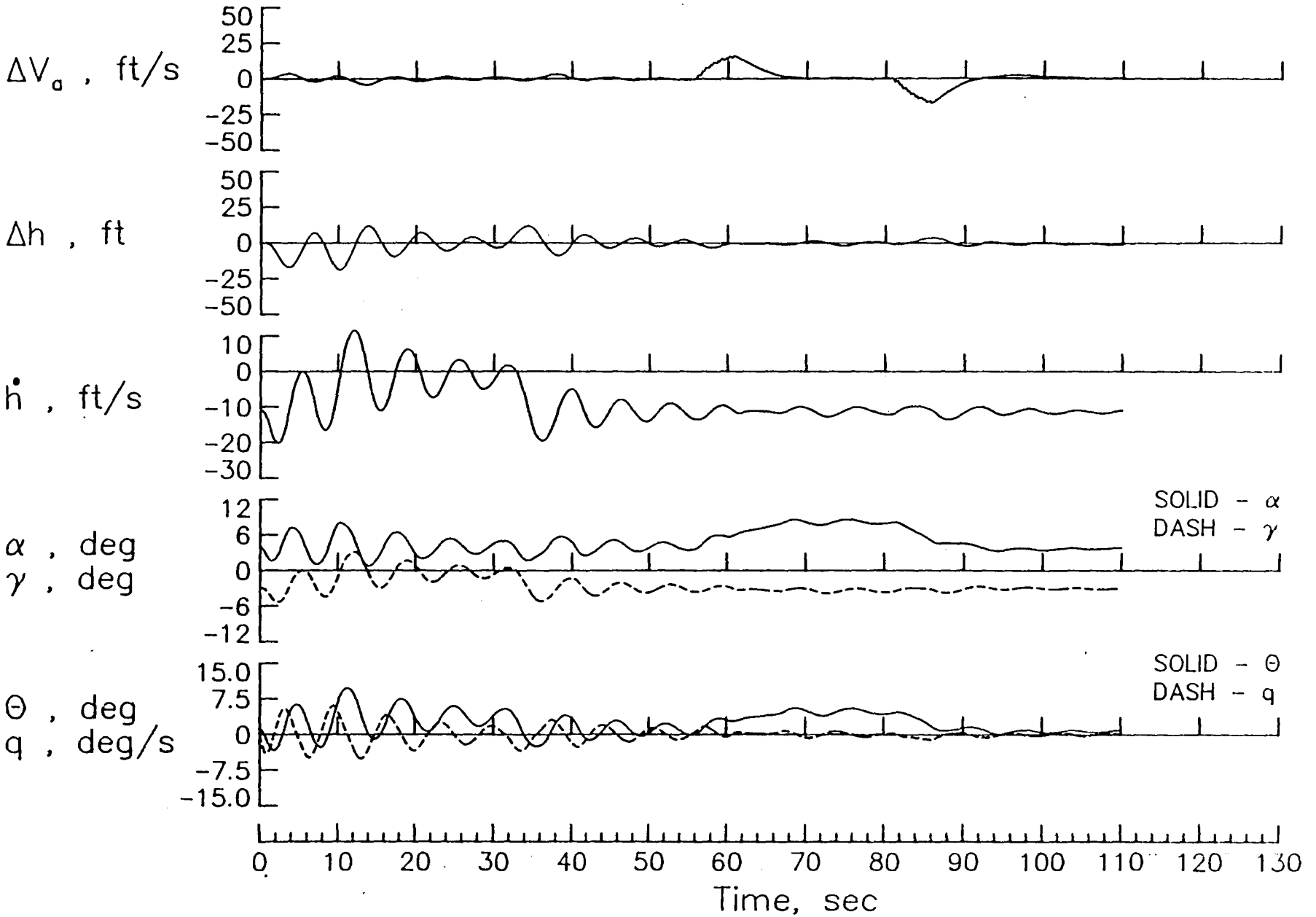

Figure 3 - CGT, δ_e failure at 10 degrees, no reconfiguration.

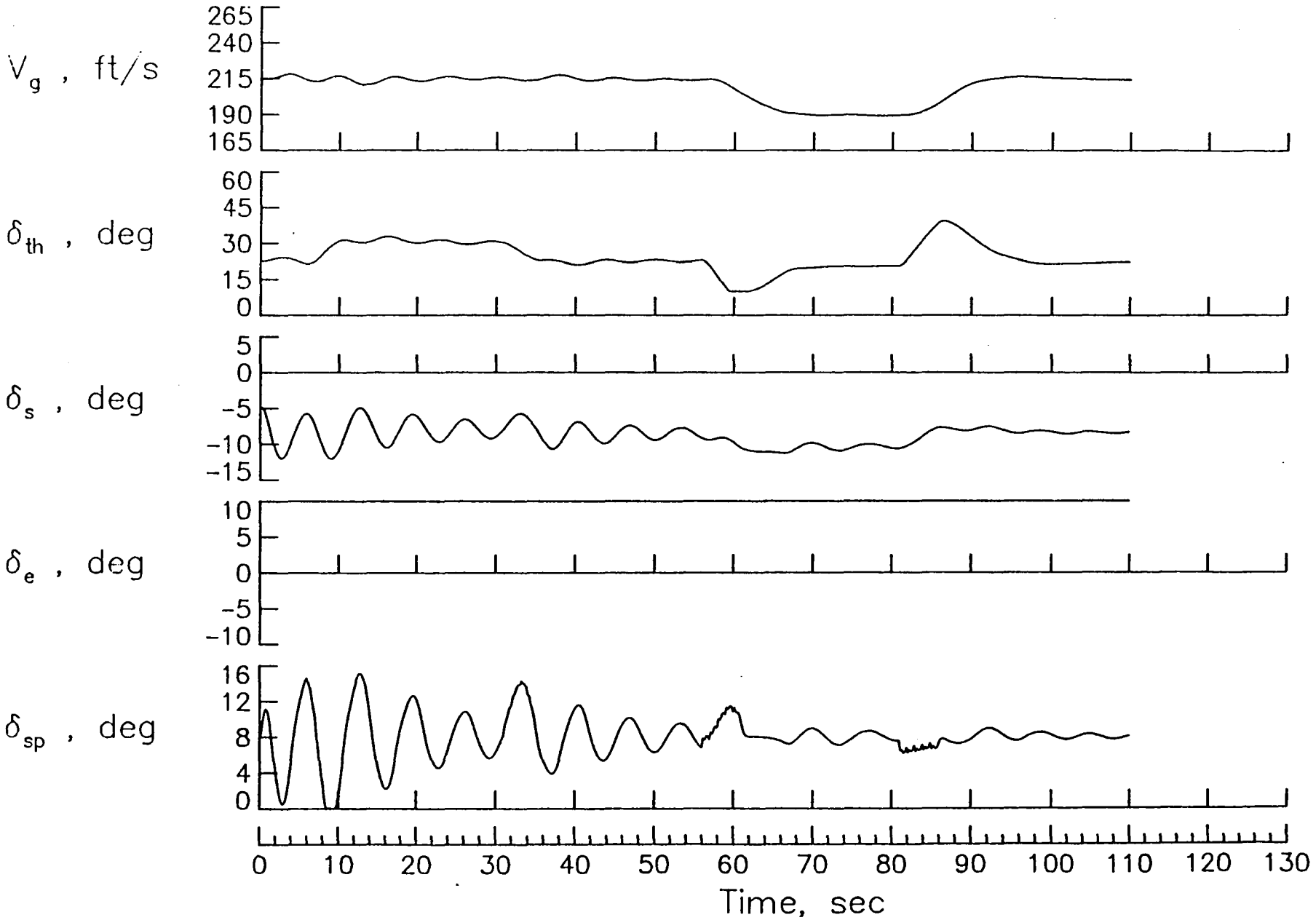

Figure 3 - concluded.

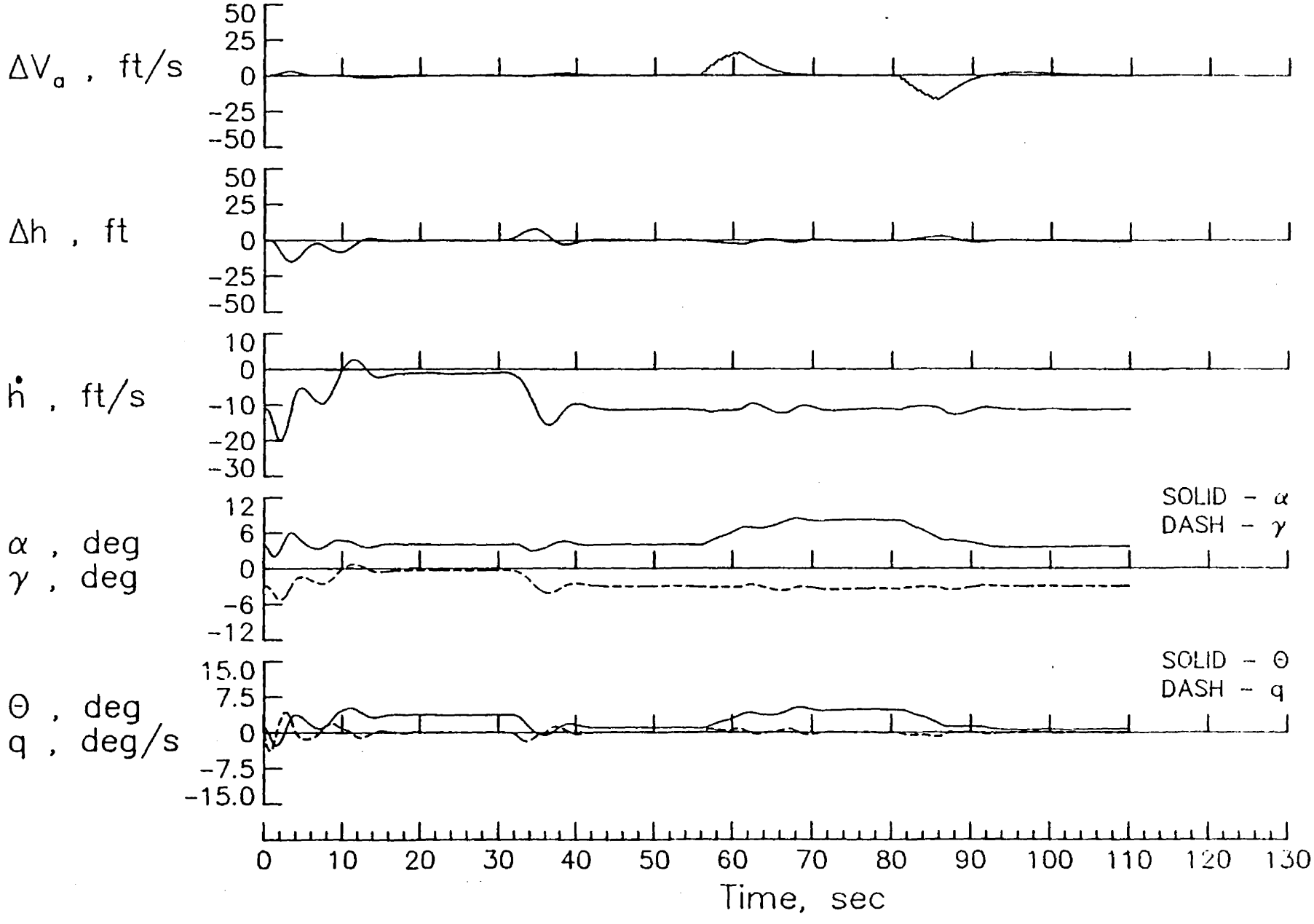

Figure 4 - CGT, δ_e failure at 10 degrees, reconfigured.

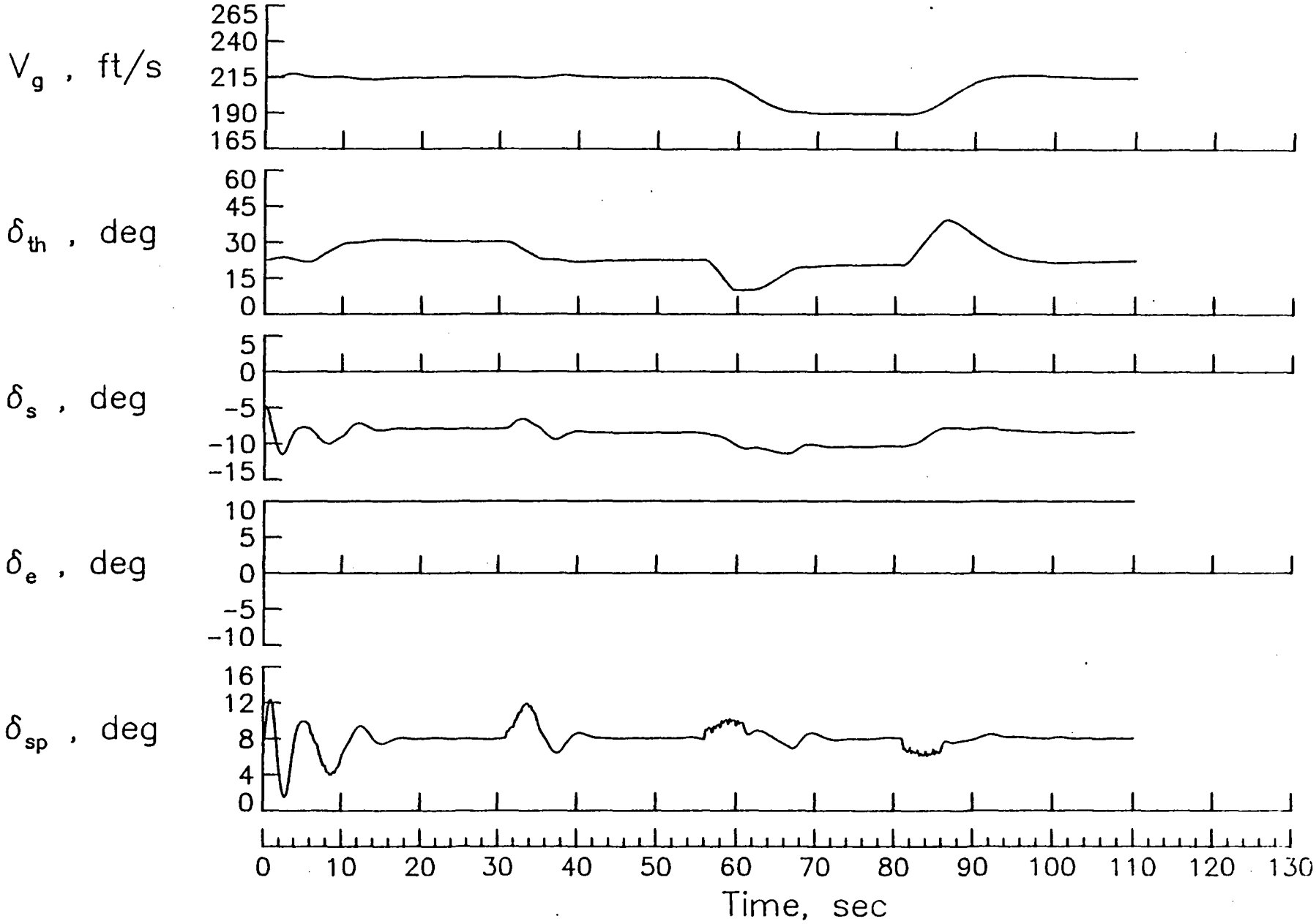

Figure 4 - concluded.

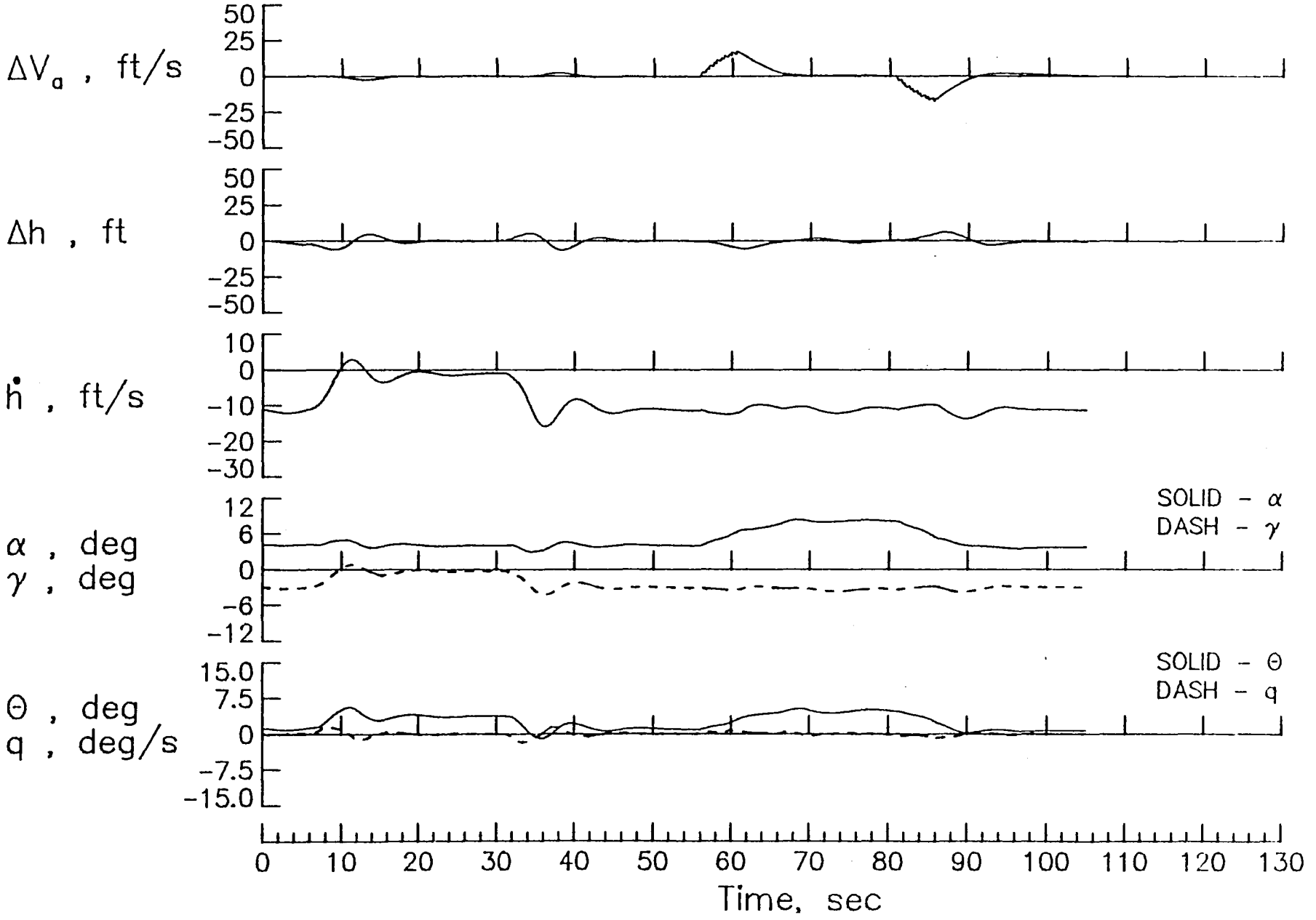

Figure 5 - CGT, δ_s failure at neutral.

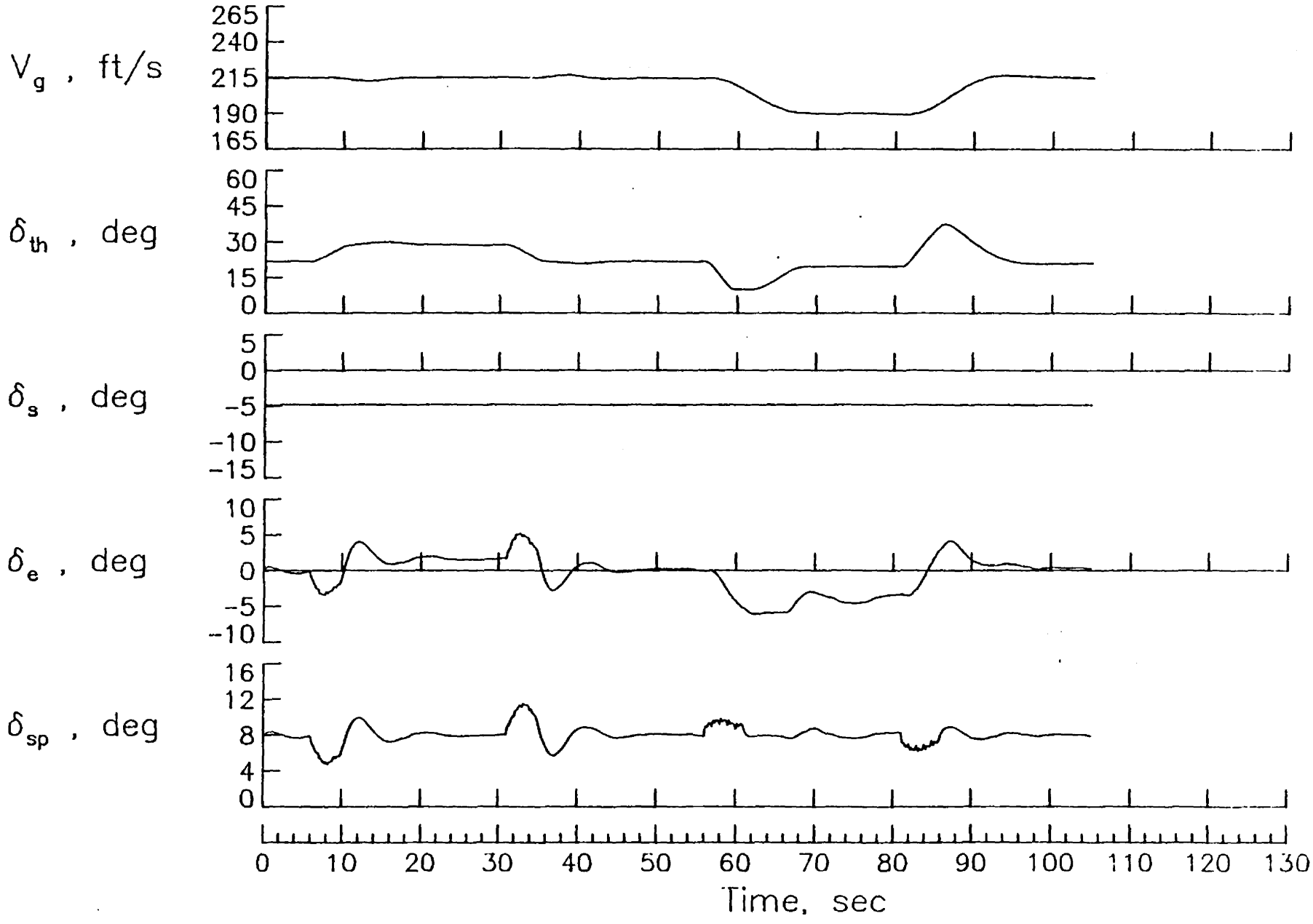

Figure 5 - concluded.

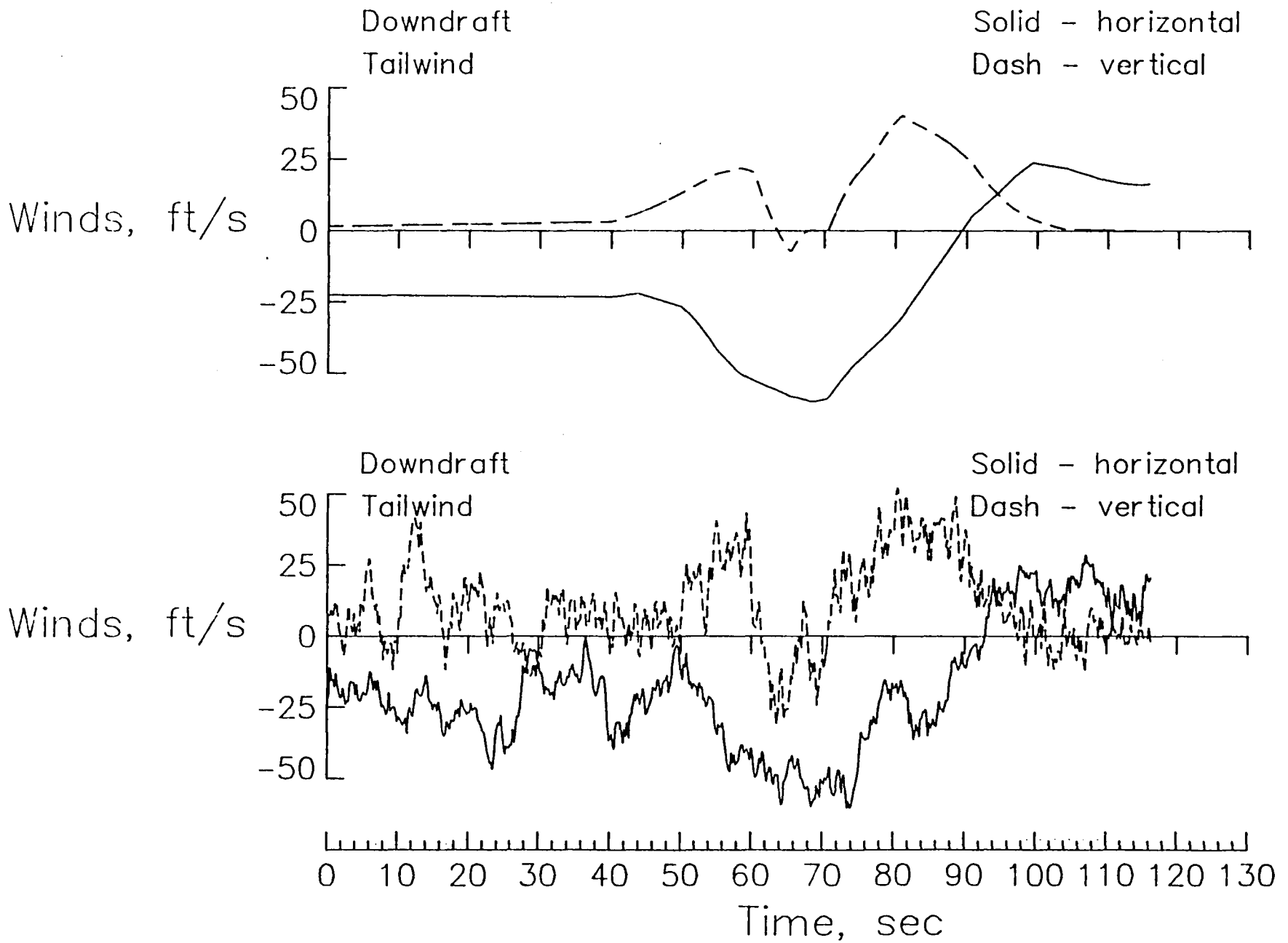

Figure 6 - SRI, Kennedy windshear and turbulence.

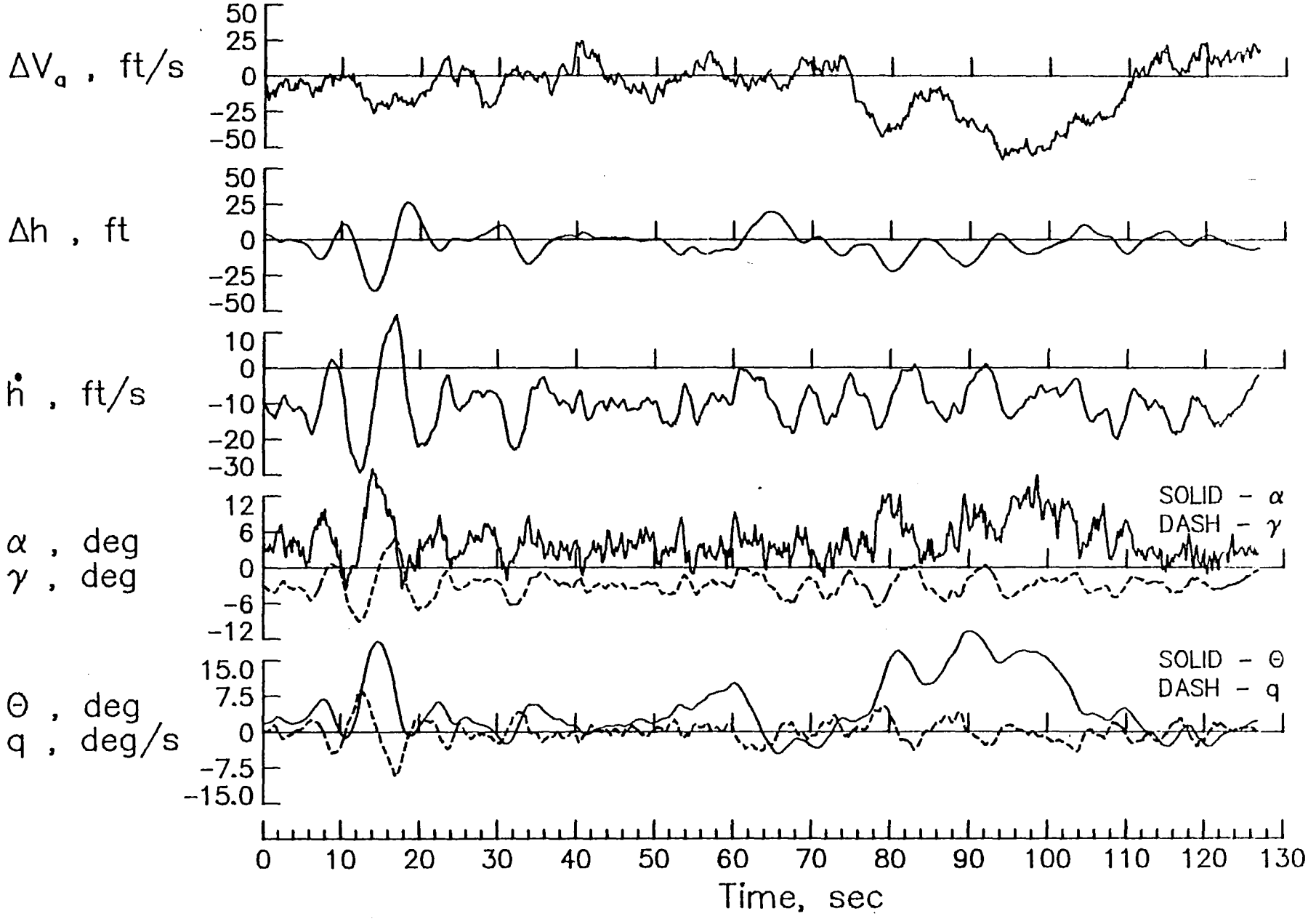

Figure 7 - 4 controls design, Kennedy windshear, velocity feedback on V_a.

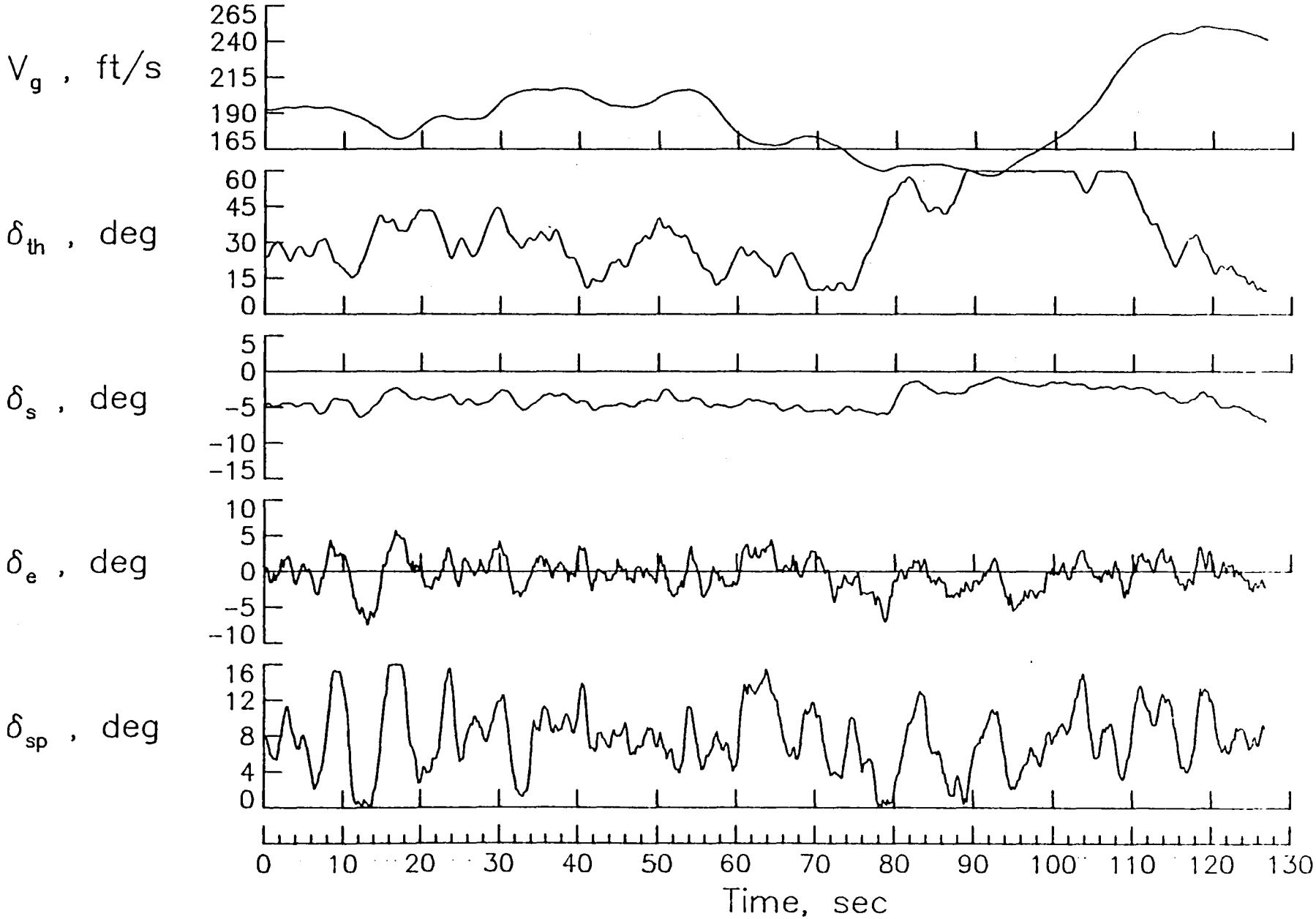

Figure 7 - concluded.

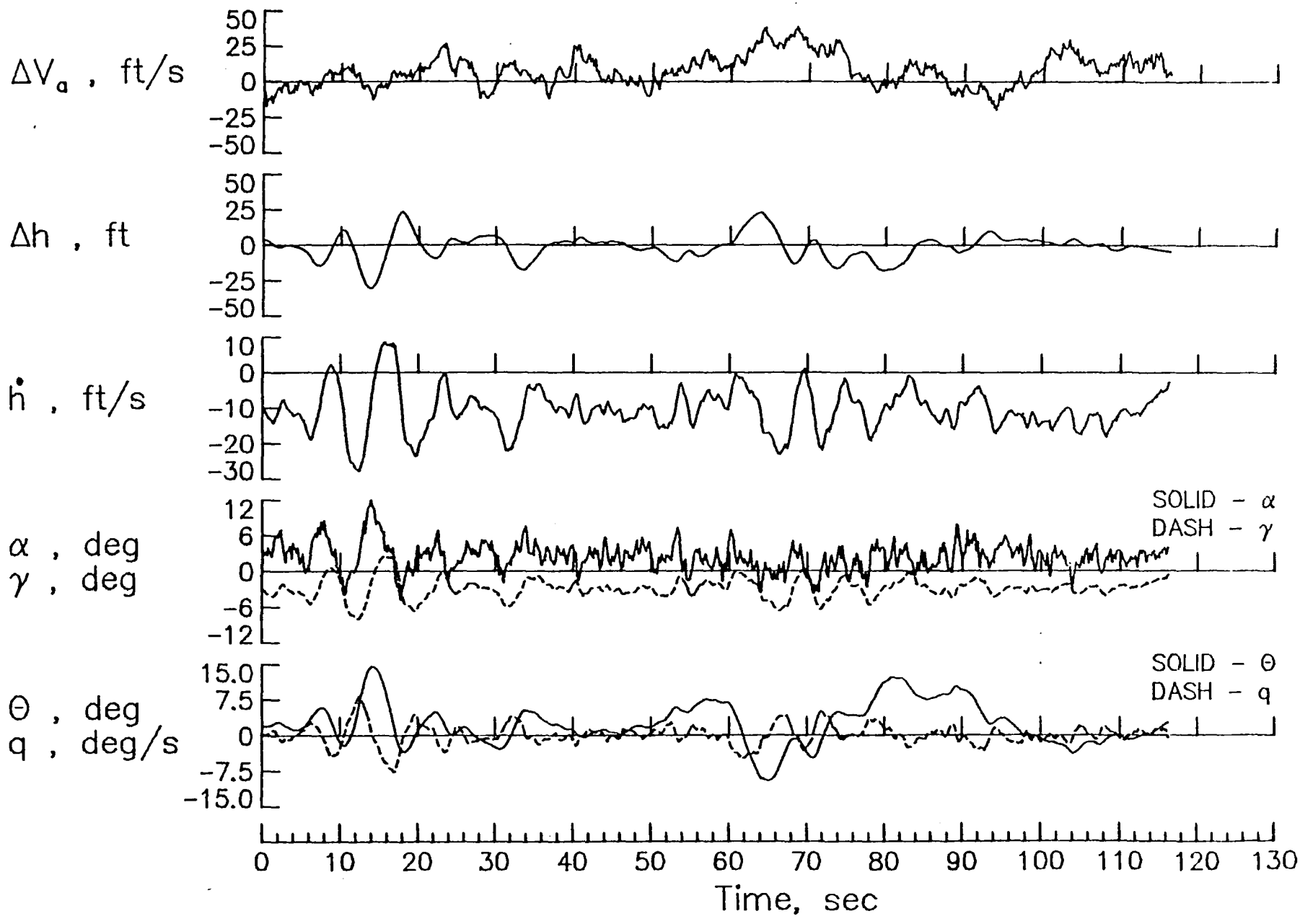

Figure 8 - 4 control design, V_a and V_g feedback, Kennedy windshear.

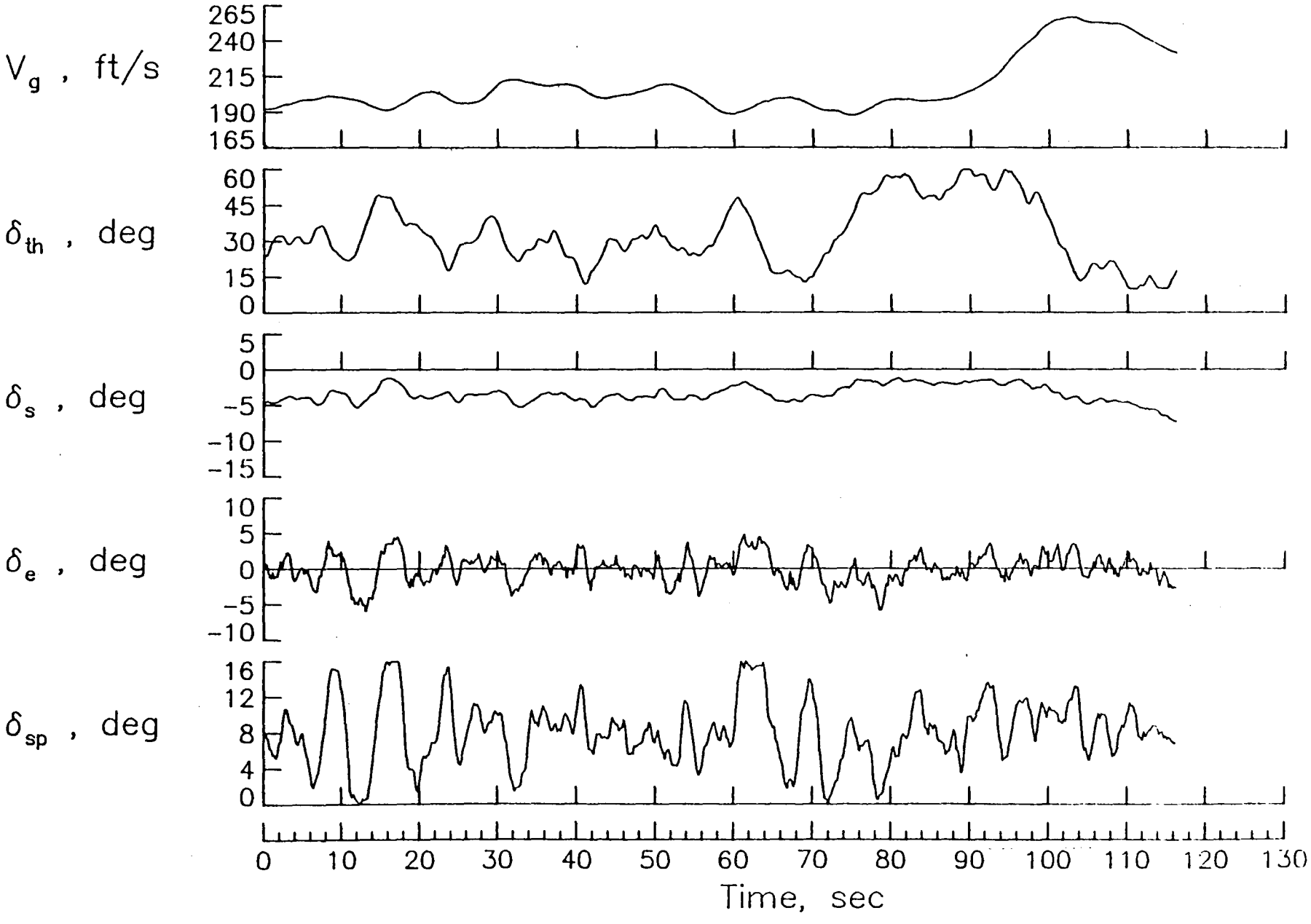

Figure 8 - concluded.

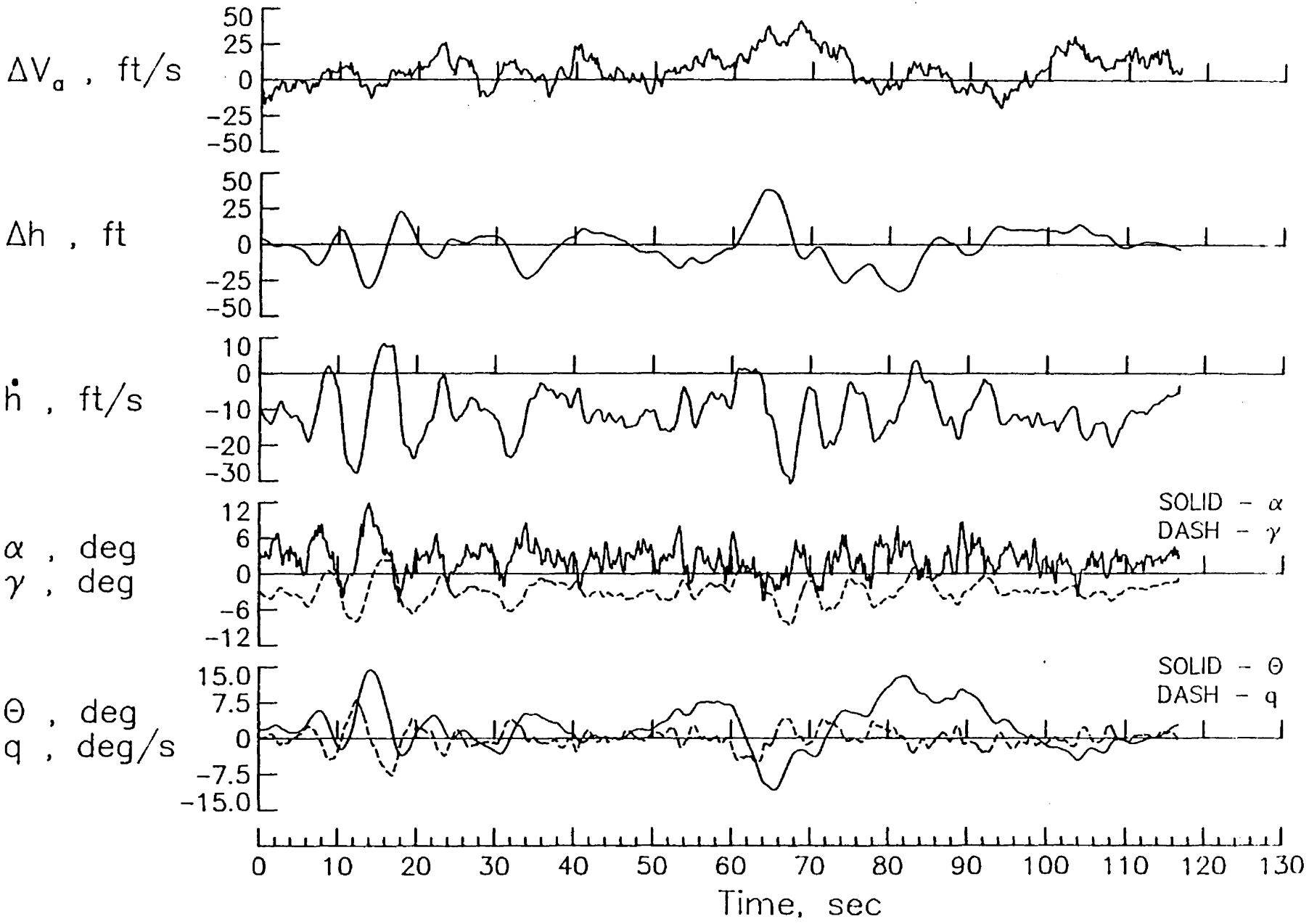

Figure 9 - δ_{sp} failed at 8 degrees, Kennedy windshear.

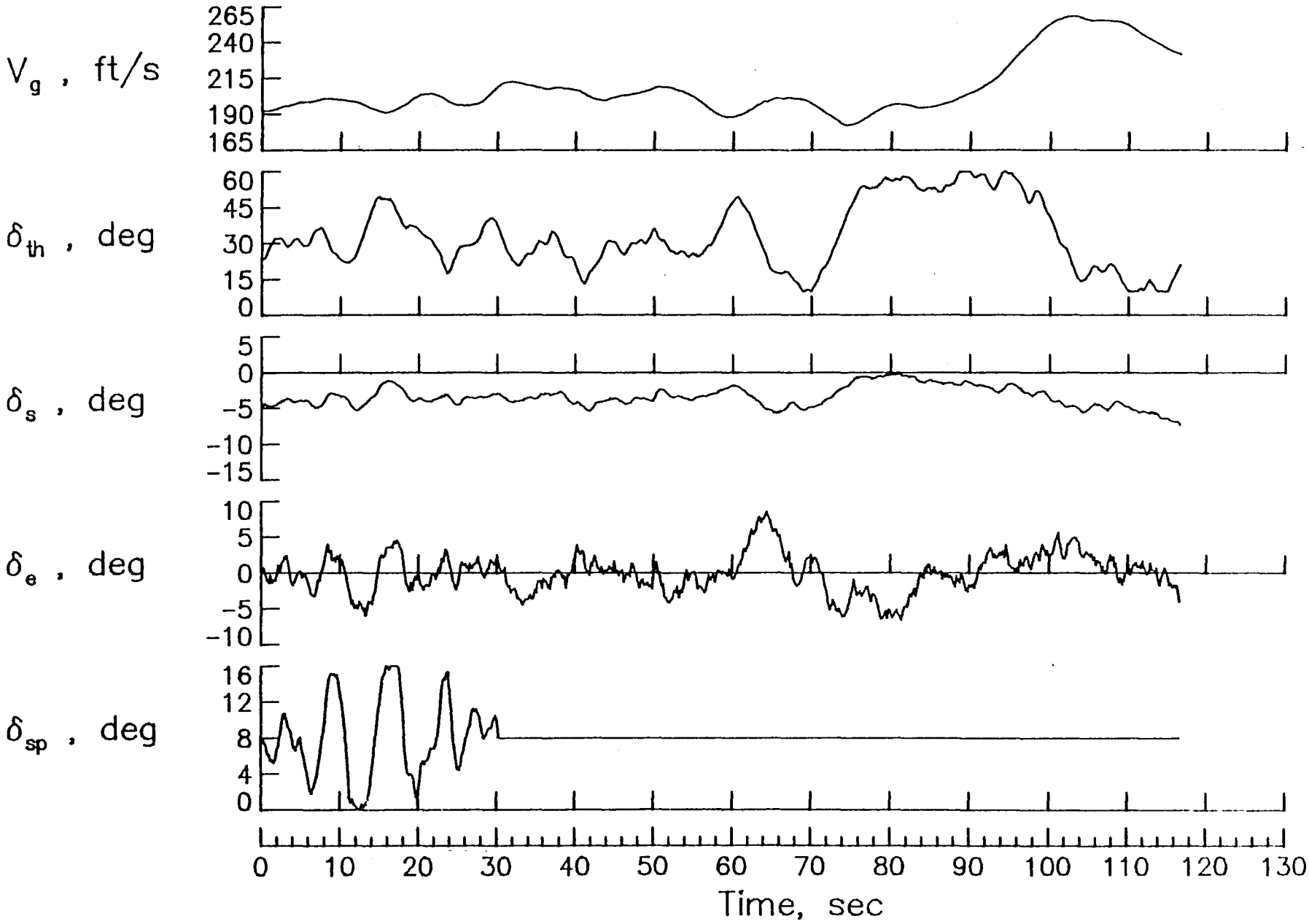

Figure 9 - concluded.

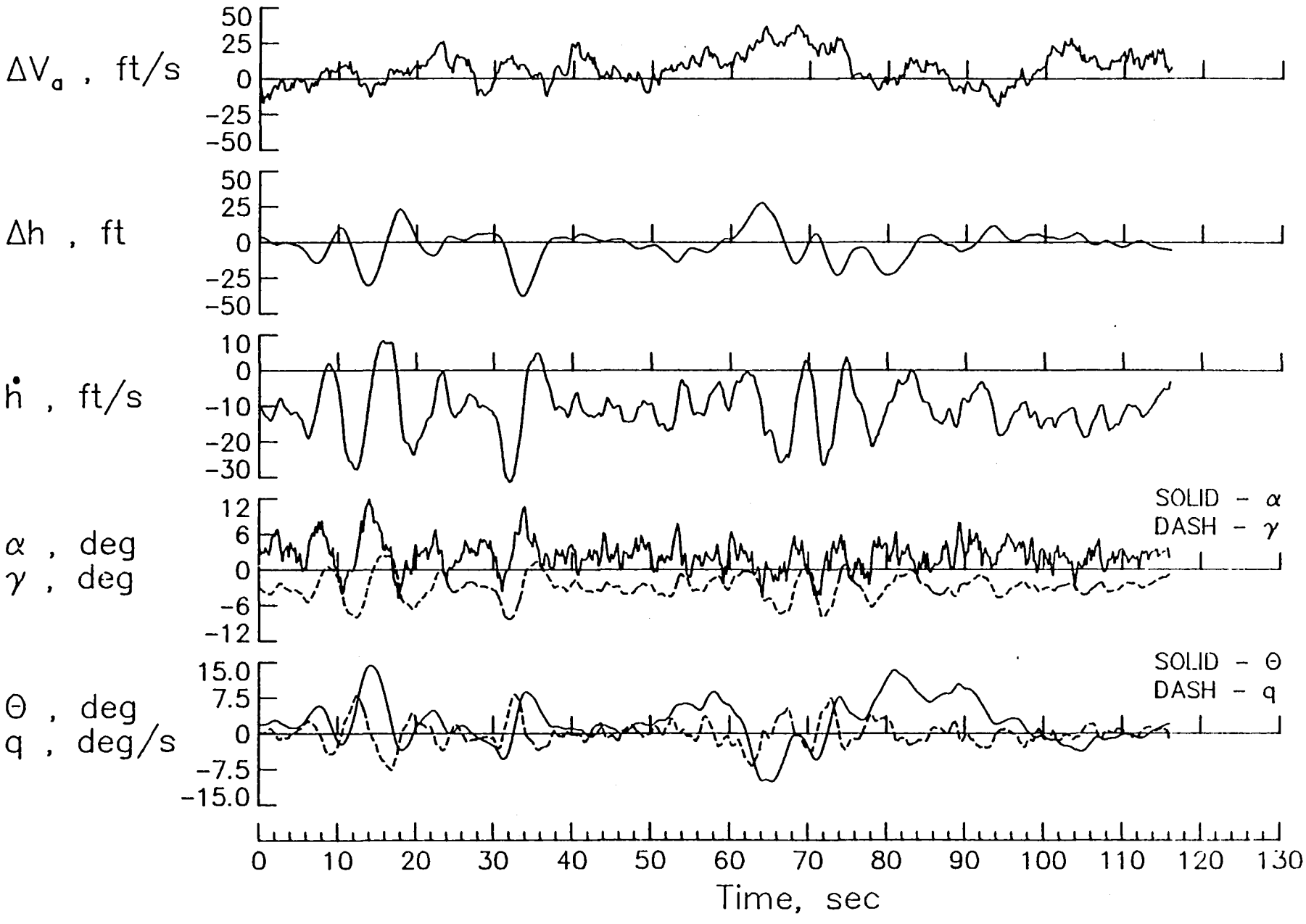

Figure 10 - δ_e failed at 10 degrees, Kennedy windshear.

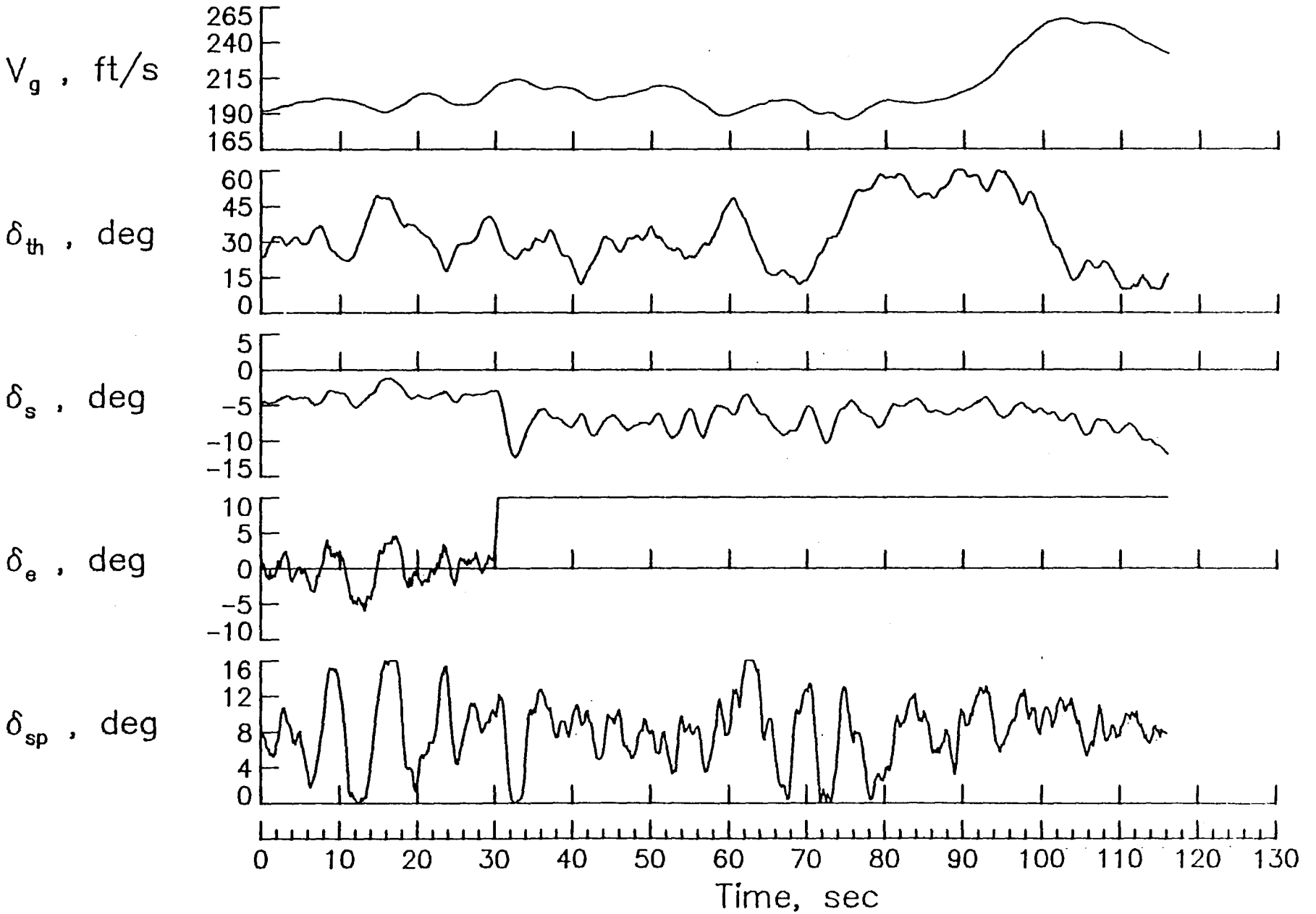

Figure 10 - concluded.

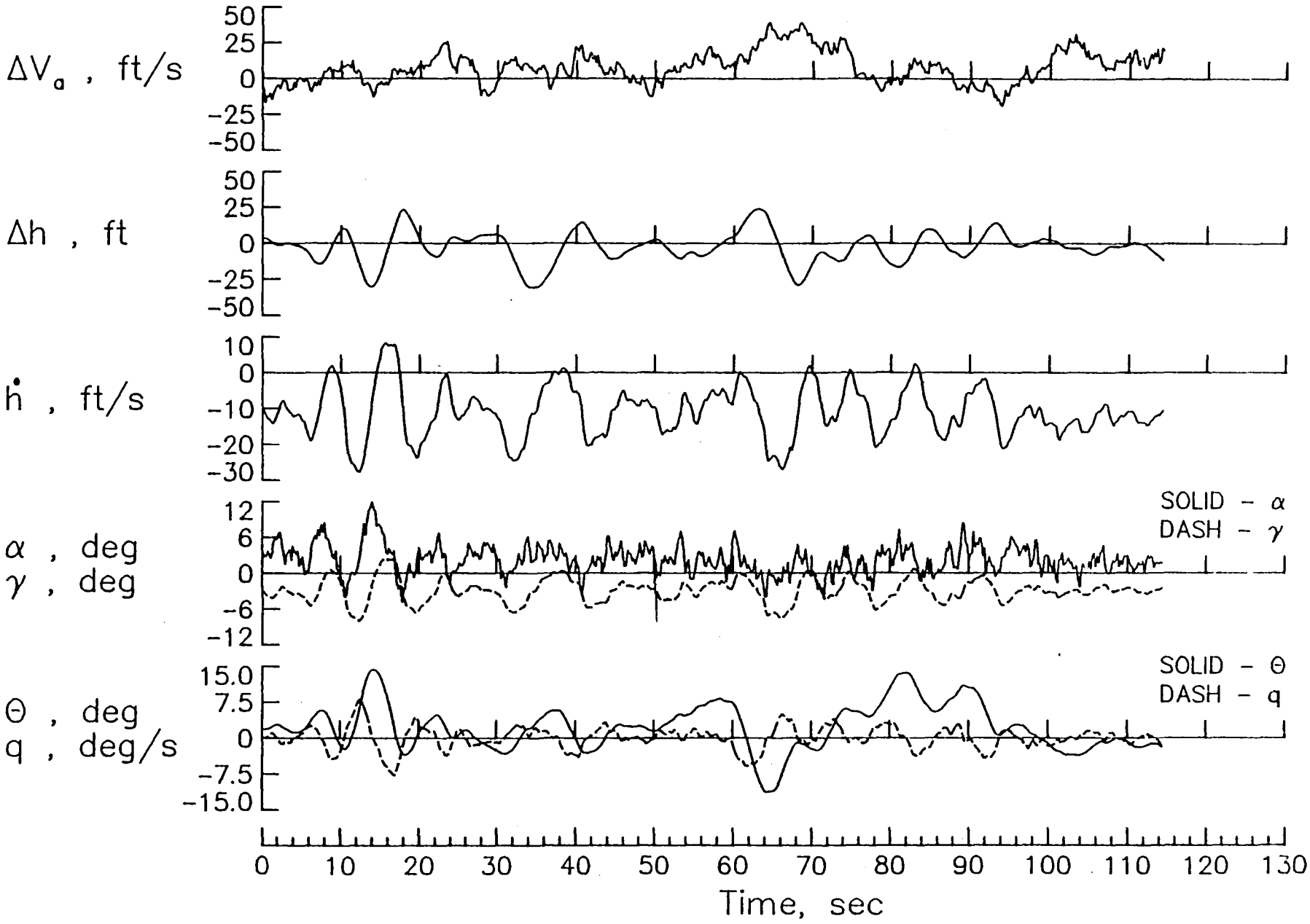

Figure 11 - δ_s failed at -2 degrees, Kennedy windshear.

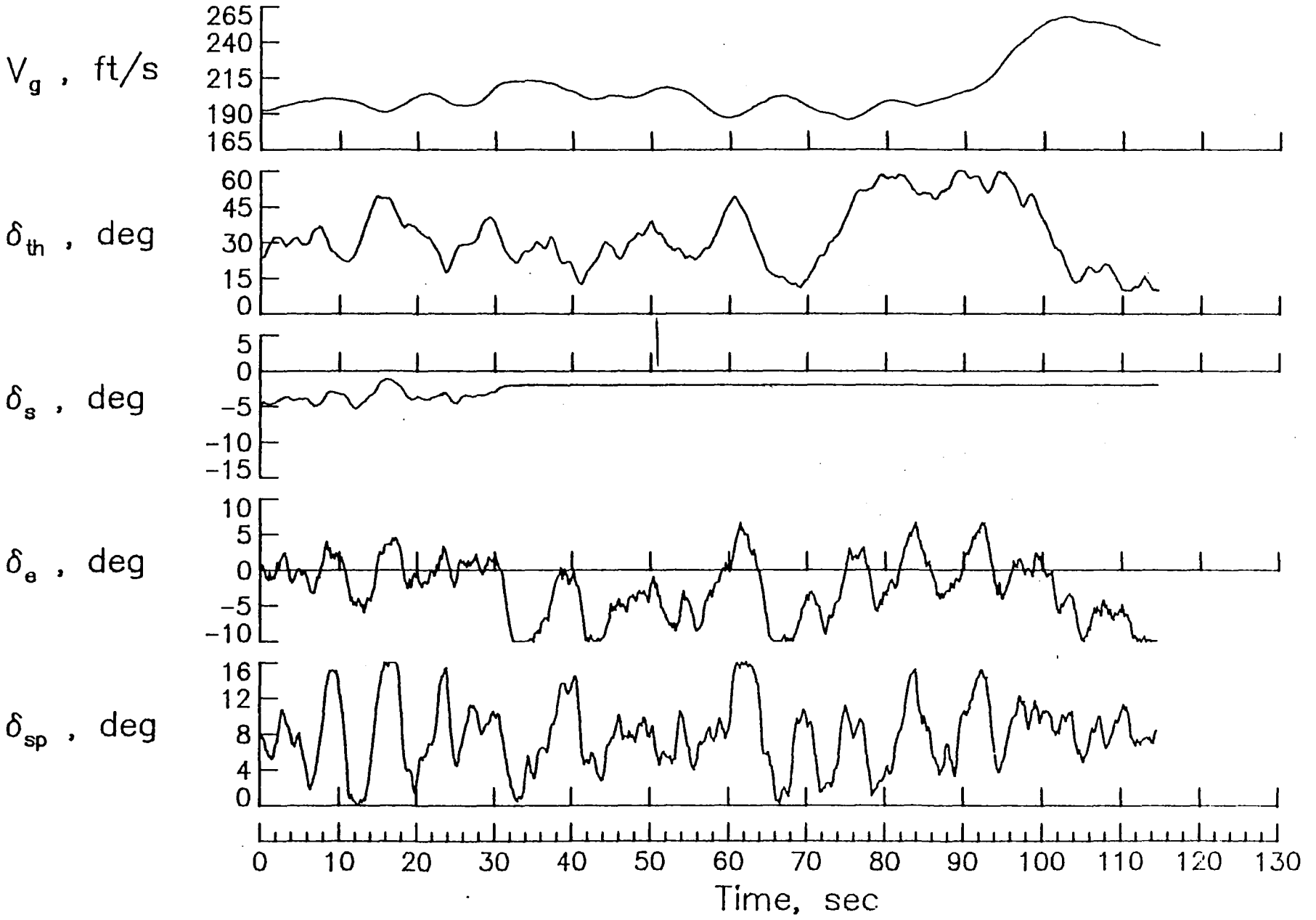

Figure 11 - concluded.

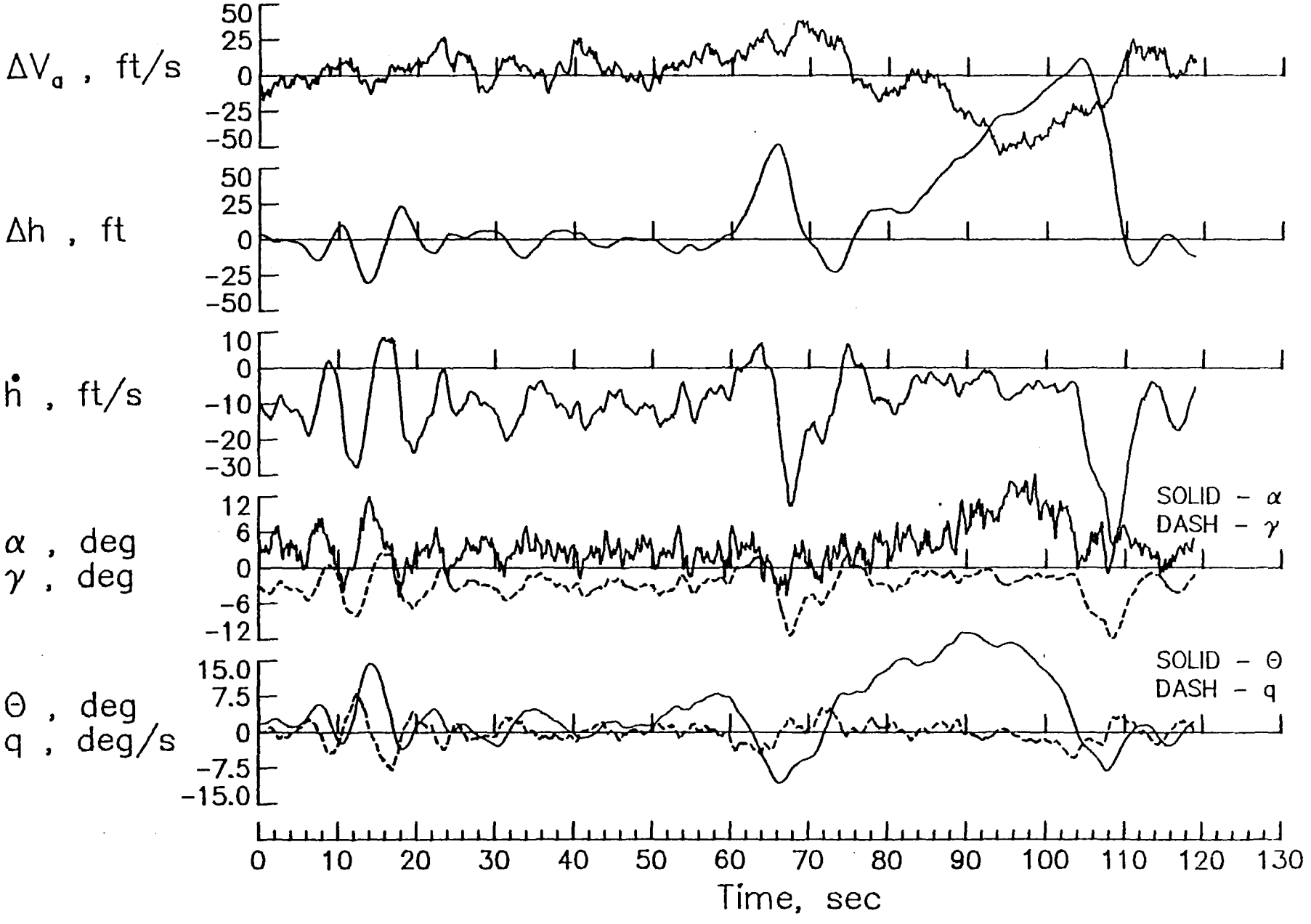

Figure 12 - δ_s failed at -5.5 degrees, Kennedy windshear.

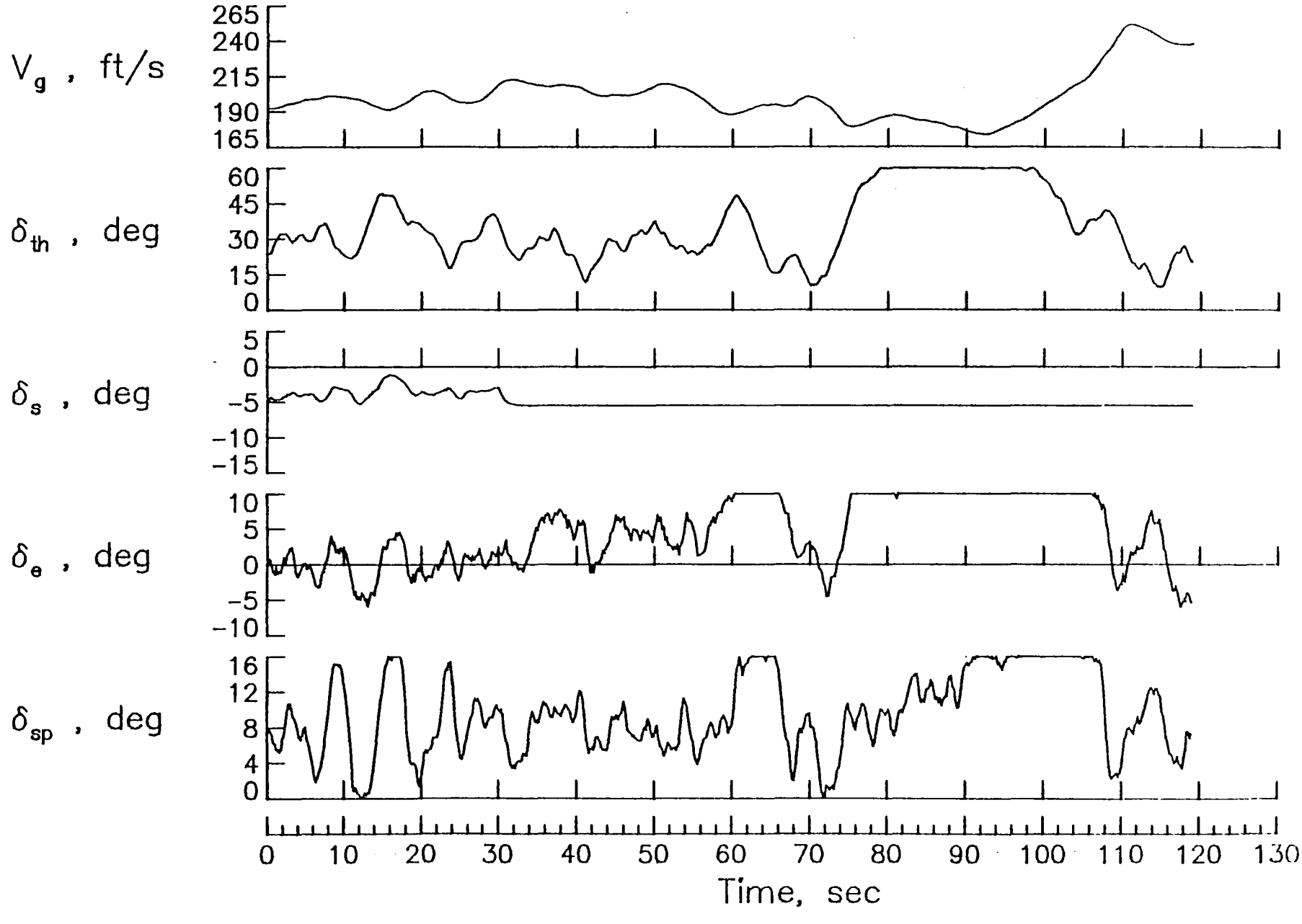

Figure 12 - concluded.

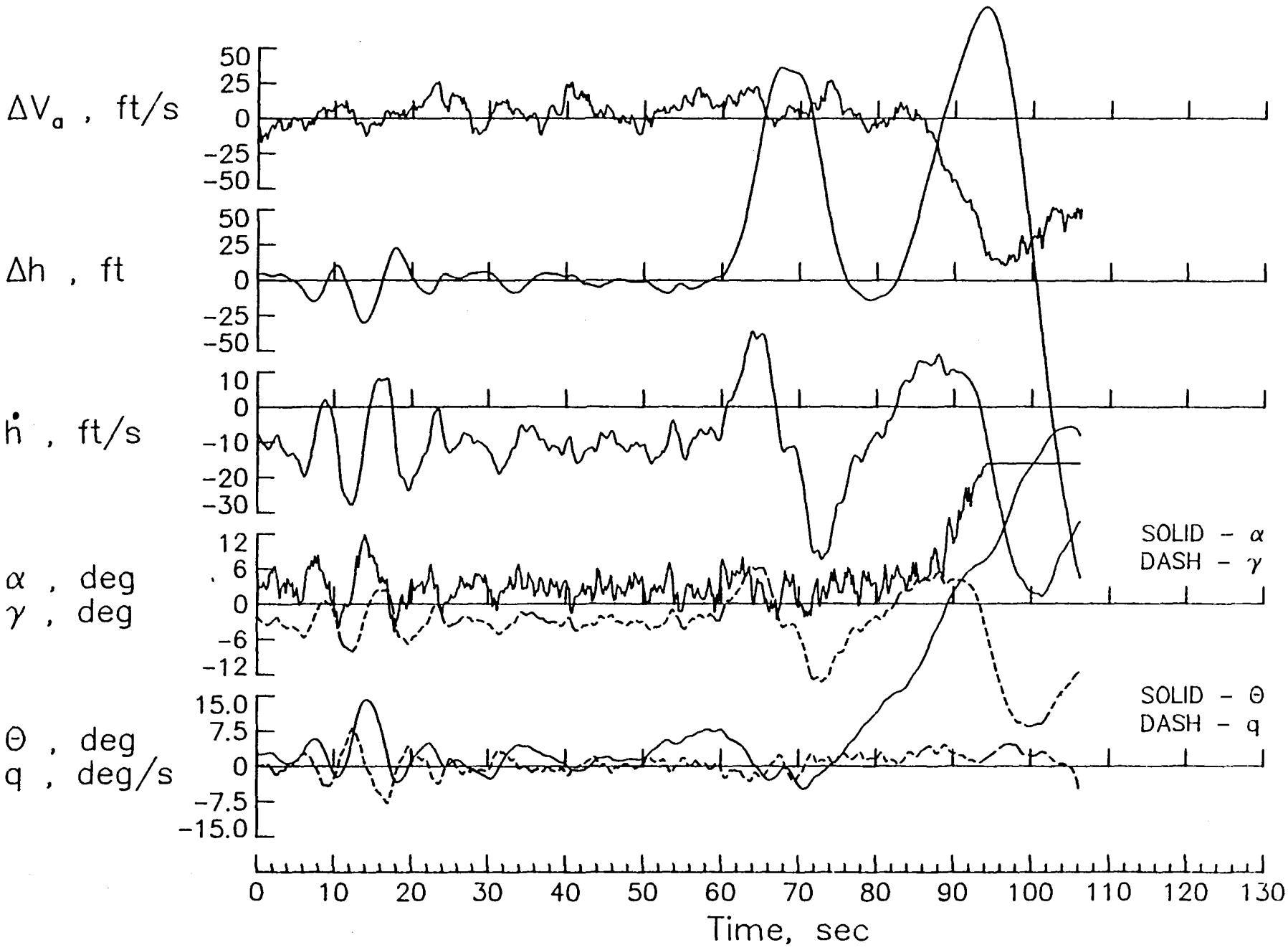

Figure 13 - δ_s failed at -6.5 degrees, Kennedy windshear.

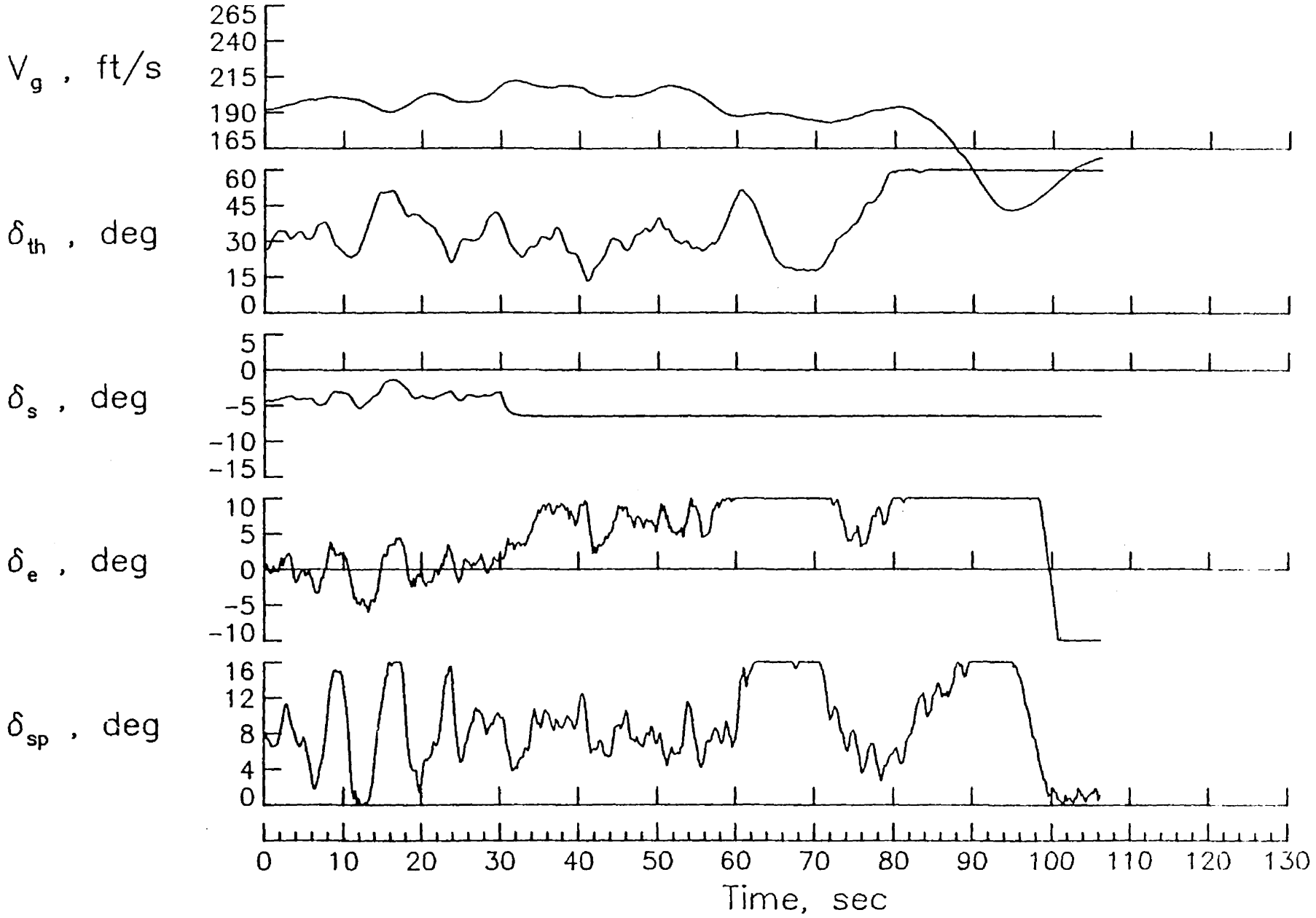

Figure 13 - concluded.

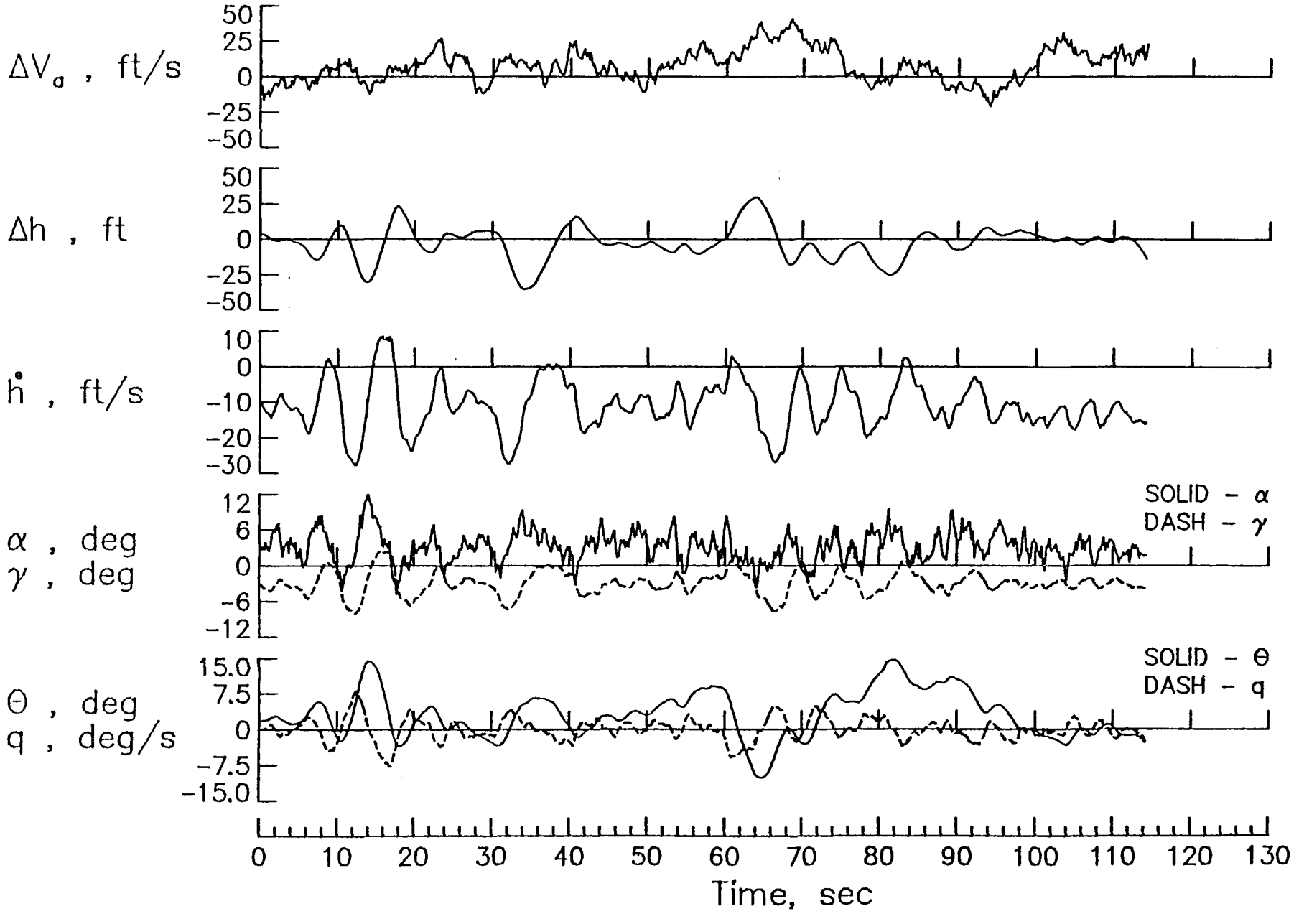

Figure 14 - 3 controls design, δ_s failed at -1 degree, δ_{sp} commanded to 12 degrees, Kennedy windshear.

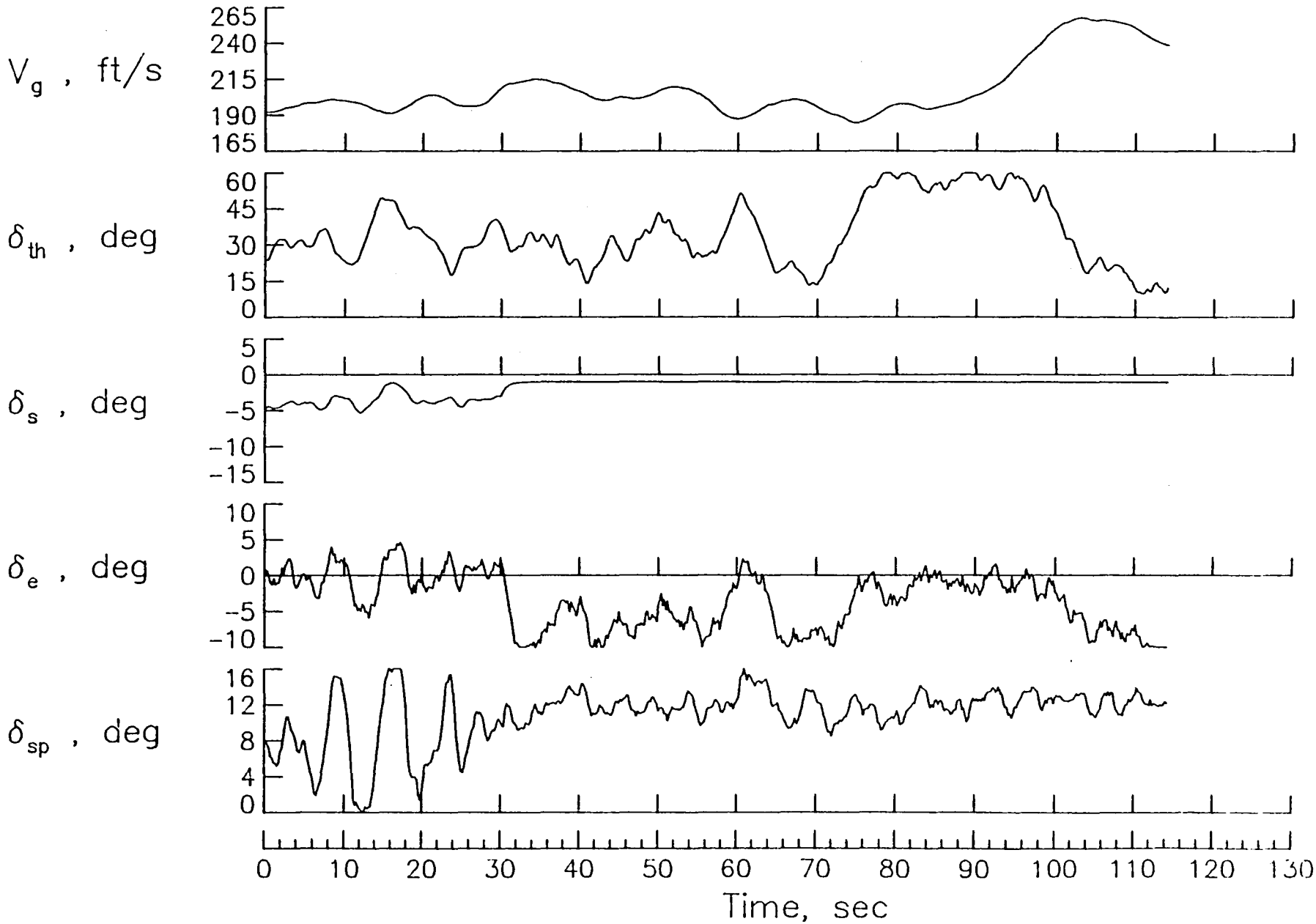

Figure 14 - concluded.

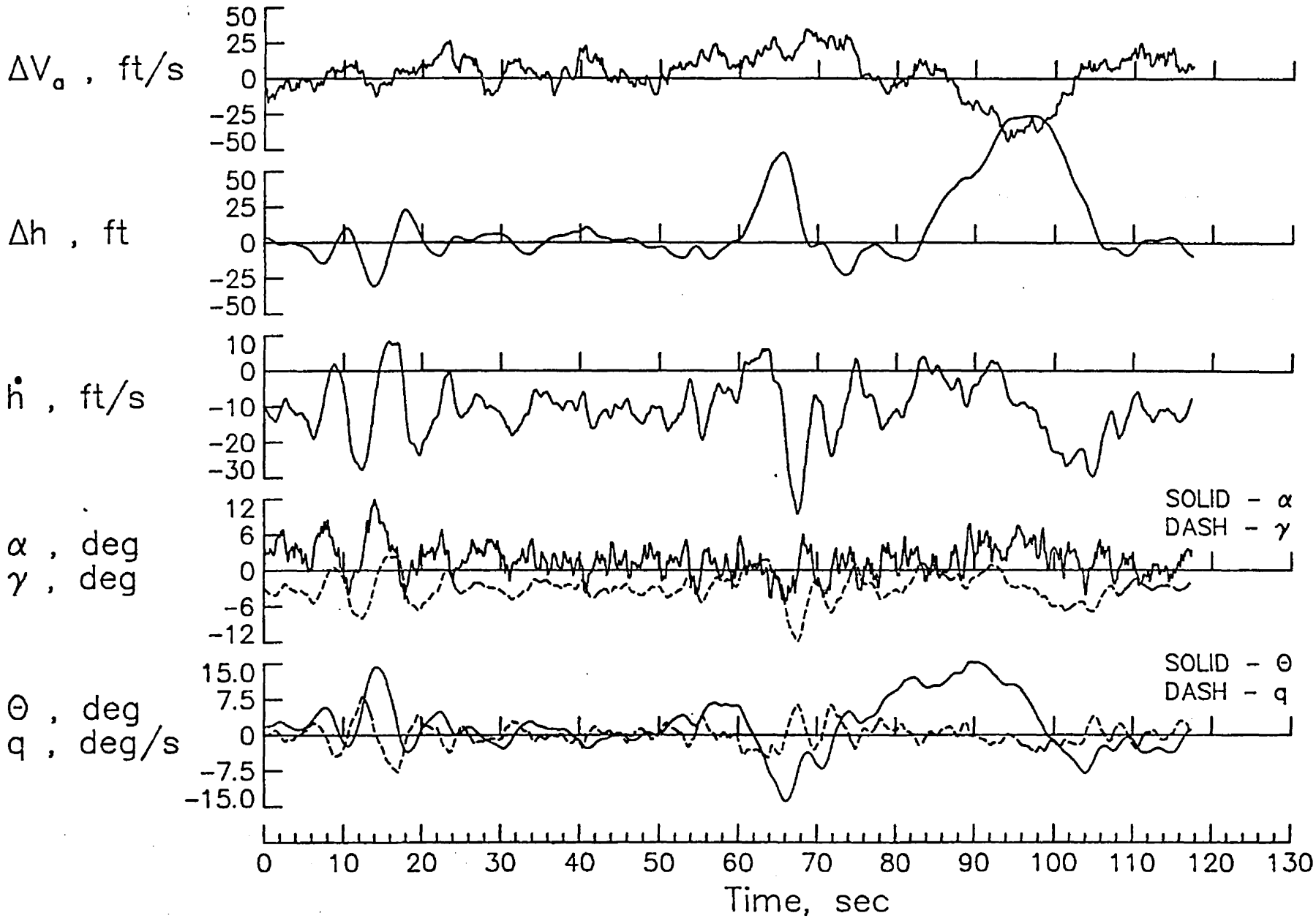

Figure 15 - 3 controls design, δ_s failed at -6.5 degrees, δ_{sp} commanded to 0 degrees, Kennedy windshear.

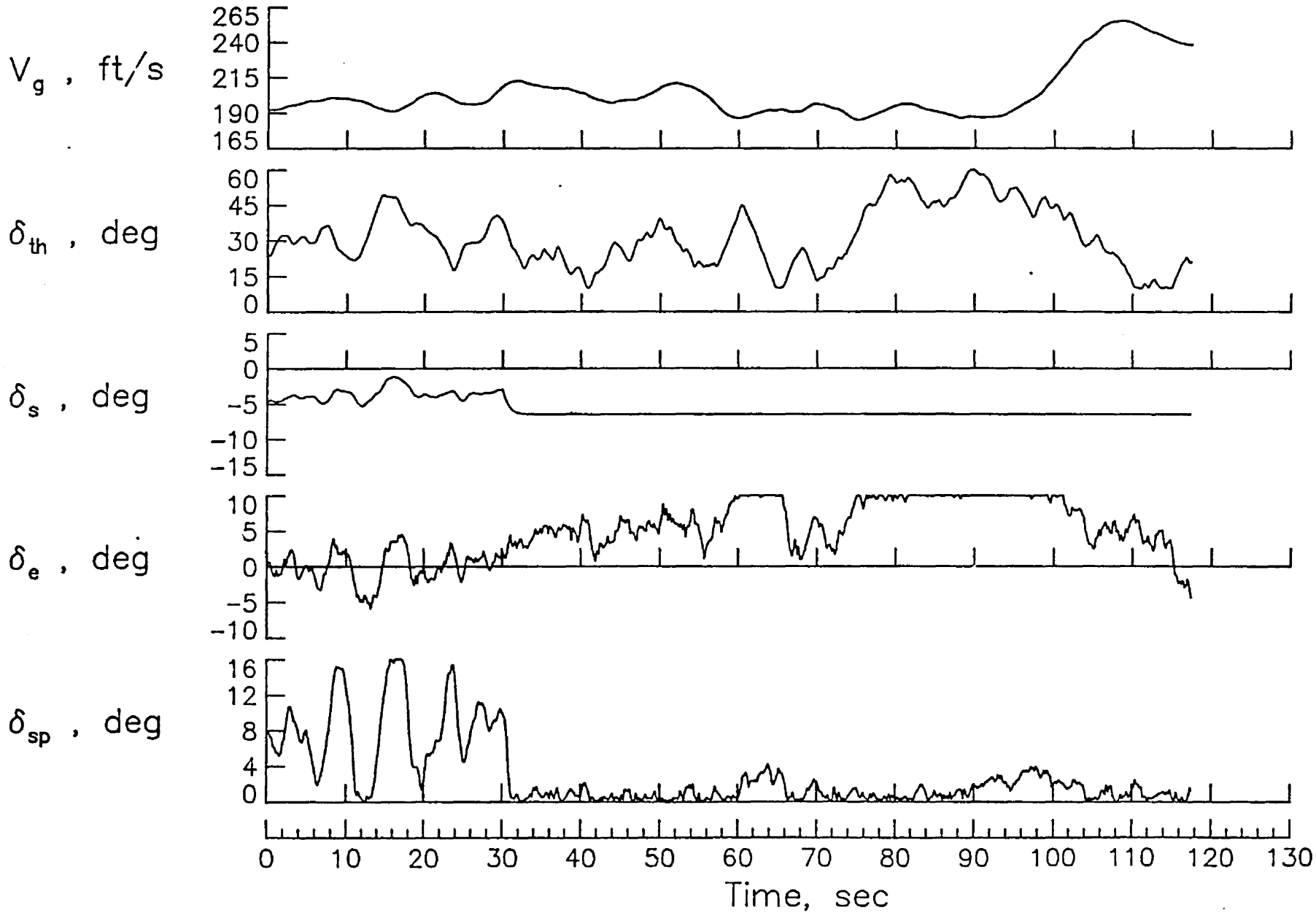

Figure 15 - concluded.

1. Report No.	2. Government Accession No.	3. Recipient's Catalog No.
NASA TM-85759		

4. Title and Subtitle	5. Report Date
Reconfigurable Multivariable Control Law for Commercial Airplane Using A Direct Digital Output Feedback Design	February 1984
	6. Performing Organization Code: 505-34-13-10

7. Author(s)	8. Performing Organization Report No.
Aaron J. Ostroff and Richard M. Hueschen	
	10. Work Unit No.
9. Performing Organization Name and Address	
NASA Langley Research Center Hampton, VA 23665	11. Contract or Grant No.
	13. Type of Report and Period Covered: Technical Memorandum
12. Sponsoring Agency Name and Address National Aeronautics and Space Administration Washington, DC	14. Sponsoring Agency Code

15. Supplementary Notes

16. Abstract

The ability of a pilot to reconfigure the control surfaces on an airplane after a failure, allowing the airplane to recover to a safe condition for landing, becomes more difficult with increasing airplane complexity. Techniques are needed to stabilize and control the airplane immediately after a failure, allowing the pilot time to make longer range decisions. This paper shows a design of a discrete multivariable control law using four controls for the longitudinal channel of a B-737. Single control element failures are allowed in three of the four controls. The four controls design and failure cases are analyzed by means of a digital airplane simulation, with regard to tracking capability and ability to overcome severe windshear and turbulence during the approach and landing phase of flight.

17. Key Words (Suggested by Author(s))	18. Distribution Statement
Reconfiguration Restructurable Control Multivariable Control Commercial Airplane	Unclassified - Unlimited Subject Category 08

19. Security Classif. (of this report)	20. Security Classif. (of this page)	21. No. of Pages	22. Price
Unclassified	Unclassified	55	A04

For sale by the National Technical Information Service, Springfield, Virginia 22161